Seasonality of archaeal lipid flux and GDGT-based thermometry in sinking particles of high latitude oceans: Fram Strait (79° N) and Antarctic Polar Front (50° S)

Eunmi Park[1,2,3], Jens Hefter[1], Gerhard Fischer[2,3], Morten H. Iversen[1,2], Simon Ramondenc[1,2], Eva-Maria Nöthig[1], Gesine Mollenhauer[1,2,3]

[1]Alfred-Wegener-Institute, Helmholtz-Center for Polar and Marine Sciences, D-27570 Bremerhaven, Germany
[2]MARUM Centre for Marine Environmental Sciences, University of Bremen, D-28334 Bremen, Germany
[3]Department of Geosciences, University of Bremen, D-28334 Bremen, Germany

Correspondence to: Eunmi Park (eunmi.park@awi.de)

Abstract The relative abundance of individual archaeal membrane lipids, namely of glycerol dialkyl glycerol tetraethers (GDGTs) with different number of cyclopentane rings, varies with temperature, which enabled their use as paleotemperature proxy index. The first GDGT-based index in marine sediments called TEX_{86} is believed to reflect mean annual sea surface temperature (maSST). The TEX_{86}^L is an alternative temperature proxy for ´low´ temperature regions (<15 ℃), where the original TEX_{86} proxy calibration shows a larger scatter. However, TEX_{86}^L-derived temperatures still display anomalous estimates in polar regions. In order to elucidate the potential cause of the disagreement between TEX_{86}^L estimate and SST, we analyzed GDGT fluxes and TEX_{86}^L-derived temperatures in sinking particles collected with time-series sediment traps in high northern and southern latitude regions. At 1296 m depth in the eastern Fram Strait (79° N), a combination of various transporting mechanisms for GDGTs might result in seasonally different sinking velocities for particles carrying these lipids, resulting in strong variability in the TEX_{86}^L signal. The similarity of flux weighted TEX_{86}^L temperatures from sinking particles and surface sediments implies an export of GDGTs without alteration in the Fram Strait. The estimated temperatures correspond to temperatures in water depths of 30−80 m, where nitrification might occur, indicating the favorable depth habitat of Thaumarchaeota. In the Antarctic Polar Front of the Atlantic sector (50° S), TEX_{86}^L-derived temperatures displayed warm and cold biases compared to satellite-derived SSTs at 614 m depth, and its flux-weighted mean signal differs from the deep signal at 3196 m. TEX_{86}^L-derived temperatures at 3196 m depth and the surface sediment showed up to 7 ℃ warmer temperatures relative to satellite-derived SST. Such a warm anomaly might be caused by GDGT contributions from Euryarchaeota, which are known to dominate archaeal communities in the circumpolar deep water of the Antarctic Polar Front. The other reason might be that a linear calibration is not appropriate for this frontal region. Of the newly suggested SST proxies based on hydroxylated GDGTs (OH-GDGTs), only those with OH-GDGT−0 and Crenarchaeol or the ring index (RI) of OH-GDGTs yield realistic temperature estimates in our study regions, suggesting that OH-GDGTs could be applied as a potential temperature proxy in high latitude oceans.

Keywords: sinking particles, GDGT, TEX_{86}^L, Fram Strait, Antarctic Polar Front

1   Introduction

The knowledge that Thaumarchaeota, one phylum of Archaea, regulate the composition of their membrane lipids according to the surrounding water temperatures enabled the development of the paleothermometer TEX_{86} (Kim et al., 2010; Schouten

5 et al., 2002). TEX_{86} is calculated based on the relative abundance of GDGTs containing 0−3 cyclopentane (GDGT−0~3) or 4 cyclopentane and one cyclohexane (Crenarchaeol) rings (Fig. 1).

The ubiquity of Thaumarchaeota, even in the polar oceans where the widely applied $U_{37}^{k'}$ proxy for sea surface temperature (SST) reconstructions is often problematic, supports the use of TEX_{86} in high latitude regions (Bendle and Rosell-Melé, 2004; Ho et al., 2014). Nonetheless, the SST dependence of TEX_{86} in warm regions is stronger than in colder regions where

10 SSTs are below 5 ℃ (Kim et al., 2010). Thus, a logarithmic calibration of TEX_{86}^L, excluding the Crenarchaeol regio-isomer, was suggested for regions where maSSTs are below 15 ℃ (see Eq. 2; Kim et al., 2010). The authors speculated that the lack of correlation between the Crenarchaeol regio-isomer and SST at low temperatures might be caused by genetically different GDGT producers. Moreover, all TEX_{86}^L calibrations for temperature include a rather large scatter, resulting in a calibration error of, e.g., ±4℃ for the TEX_{86}^L calibration (Kim et al., 2010).

15 It has been questioned whether temperature is the only factor influencing the lipid composition (i.e., TEX_{86}) particularly in the regions where strong cold or warm biases were observed between TEX_{86} reconstructed and measured maSSTs. The biases of TEX_{86} calibrations have been attributed to enhanced production of GDGTs during seasons with favorable growth conditions for Thaumarchaeota (Pitcher et al., 2011; Wuchter et al., 2006b), a contribution of GDGTs from deep dwelling communities (Kim et al., 2015; Lee et al., 2008; Taylor et al., 2013), terrestrial input (Weijers et al., 2006), influences of

20 different archaeal communities (Lincoln et al., 2014; Turich et al., 2007), and/or other environmental factors (Huguet et al., 2006; Mollenhauer et al., 2015; Park et al., 2018; Turich et al., 2007).

To circumvent these problems, especially in cold regions, a handful of studies have developed dedicated calibrations on regional scales (Meyer et al., 2016; Seki et al., 2014; Shevenell et al., 2011). For the temperature estimate in the Eocene Arctic Ocean, a modified version of TEX_{86}, the index termed TEX'_{86} was proposed (Sluijs et al., 2006). It excludes

25 GDGT−3 to eliminated contribution from terrestrial input, leading to significantly higher temperature estimates compared to the original TEX_{86} calibration. The TEX'_{86} values of 104 marine surface sediments showed a good linear correlation with maSSTs ($R^2 = 0.93$) (Sluijs et al., 2006). Following the addition of 7 additional TEX_{86} values from surface sediments collected at the continental margin of the western Antarctic Peninsula, Shevenell et al., (2011) modified the Kim et al., (2008)'s TEX_{86} calibration for this region ($TEX_{86} = 0.0125 \times Temp + 0.3038$, $R^2 = 0.82$) and estimated water temperatures

30 for the Holocene.

Ho et al., (2014) evaluated TEX_{86} and the different calibrations in an extended set of surface sediments from the polar regions of both hemispheres and found that the global TEX_{86} calibration is suitable for subpolar regions (e.g., the Pacific sector of the Southern Ocean and the Subarctic Front in the North Pacific). Additionally, the TEX_{86}^L yields reasonable temperature estimates if regional calibrations are developed for high latitude regions. Using a regression of water temperatures (at 20 m depth in August) versus TEX_{86}^L values, Seki et al., (2014) obtained plausible paleotemperature estimates for the Sea of Okhotsk and the subpolar North Pacific region. Meyer et al., (2016) confirmed later that this regional TEX_{86}^L calibration can also be applied to the subarctic northwest Pacific and the Western Bering Sea.

More recently, hydroxylated GDGTs (OH-GDGTs), which contain an additional hydroxyl group in one of the biphytanyl moieties of GDGT−0, −1, and −2, have been recognized in marine sediments (Liu et al., 2012; Fig. 1). Based on the finding that the abundance of OH-GDGTs relative to the total isoprenoid GDGTs increase towards cold regions (Huguet et al., 2013), OH-GDGT based SST calibrations have been proposed for high latitude oceans (Fietz et al., 2013; Huguet et al., 2013).

Beside the biological, phylogenetical, and statistical studies of the temperature proxy, sinking particles collected in specific regions can provide new perspectives on the distribution of GDGTs and TEX_{86} based temperature reconstructions. The study using time-series sediment traps can give insights on the seasonal variability of lipid flux and temperature signals, and allows comparing the lipid signal to those in underlying sediments. Only one TEX_{86} study using a time-series sediment trap in high latitude regions has been conducted near Iceland (Rodrigo-Gámiz et al., 2015), regardless of the interest in polar regions, where temperature reconstructions with lipid proxies are troublesome. Here, we examine the seasonal GDGT production and TEX_{86}^L-derived temperatures in comparison to measured SSTs in order to better understand the drivers influencing TEX_{86}^L values in sinking particles collected in two high latitude oceans (eastern Fram Strait, 79° N and Antarctic Polar Front of the Atlantic sector, 50° S). The temperatures derived from OH-GDGT proxies were also calculated to evaluate the applicability of these novel proxies for high latitude regions.

2   Study area

2.1   Fram Strait

The Fram Strait is located west of Spitsbergen, where the heat exchange occurs between the Arctic Ocean and the North Atlantic (Fig. 2). Relatively warm and nutrient-rich Atlantic water (AW) is transported by the West Spitsbergen Current (WSC) to the central Arctic Ocean, while colder and less saline Arctic water is transported along the East Greenland Current (EGC) to the Nordic Seas (Fig. 2). Part of the WSC is separated from the northward flow and recirculated within the region (Manley, 1995; Soltwedel et al., 2016). Eddies, mixing, and recirculating Atlantic water contribute to the hydrographic complexity observed in the Fram Strait (Walczowski, 2013). The volume transport of the WSC and AW within the WSC displays strong seasonality with maxima in March and minima in July for the WSC, and maxima in late autumn and winter and minima in June for the AW (Beszczynska-Möller et al., 2012b). The occurrence of sea ice and its variability has an

effect on the particle fluxes as well as on benthic ecosystems (Bauerfeind et al., 2009; Hebbeln and Wefer, 1991; Soltwedel et al., 2016). Sinking particles in the Fram Strait, including organic and terrigenous material, are well known to originate not only from the photic zone in the upper water column, but also from the Svalbard archipelago and Siberian shelf, from where they are transported by sea ice (Hebbeln, 2000; Lalande et al., 2016). Phytoplankton blooms enhance the vertical flux of

5 biogenic components (organic carbon, carbonate, and opal) in spring-summer, but the downward flux of particles is likely affected by the environmental conditions (e.g. hydrographic changes, sea ice extent, and atmospheric low-pressure) on an annual time scale (Wassmann et al., 2006). Based on oceanographic measurements from mooring arrays at multiple depths across the Fram Strait (from 7° W to 9° E, 78.3° N), Beszczynska-Möller et al., (2012) found two warm anomalies in the Atlantic water through the Fram Strait in 1999−2000 and 2005−2007. During the second warm anomaly, community

10 structures of phytoplankton and zooplankton were affected by the decreased sea ice in this region (Lalande et al., 2013; Nöthig et al., 2015) and had a profound influence on biogenic sediment fluxes.

2.2 Antarctic Polar Front

The Antarctic Polar Front (APF) region is one of the major frontal zones within the westerly wind driven Antarctic Circumpolar Current (ACC) (Fig. 2). Spatial and temporal variability of the APF is strongly affected by seafloor topography.

15 The APF has an average width of 43 km (1987−1993), which moves southward during the austral summer and reaches its northernmost position during the austral winter (Moore et al., 1999). The ACC is well known for its meandering jet flow and eddy formation (Moore et al., 1999; Orsi et al., 1995), which likely stimulate phytoplankton blooms and primary production in this region by supplying growths limiting nutrients, and/or bringing deeper dwelling phytoplankton into the photic zone (Abbott et al., 2001; Moore and Abbott, 2000, 2002). Thus, the hydrographic structure is an important factor controlling the

20 distribution of phytoplankton and small zooplankton in this region (Read et al., 2002). The highest chlorophyll-a levels of up to 3.5 mg m^{-3} were recorded in the APF during the early austral summer 1990−1991, and it co-occurred with elevated silicate levels as well as water column stratification (Laubscher et al., 1993). The current speed close to the PF3 trap was recorded to be up to 8 cm s^{-1} (Walter et al., 2001). Read et al., (2002) reported the vertical profile of currents measured between the surface and 400 m depth in the polar frontal regions in December 1995. The currents recorded at the surface and

25 subsurface of the Polar Front were much stronger (30−50 cm s^{-1}) than the ones measured at 700 m depth (1−8 cm s^{-1}) by Walter et al., (2001).

3   Material and Methods

3.1 Sediment Traps

A time-series sediment trap system was moored to collect sinking particles at the eastern Fram Strait (FEVI16) between July

30 2007 and July 2008 at 1296 m water depth (Table 1, Fig. 2). Two traps (PF3) were deployed in the permanent ice free-area of the APF in the Atlantic sector at 614 m and 3196 m water depth from November 1989 to December 1990 (Table 1, Fig. 2).

The cone-shaped funnel of the Kiel trap systems had a 0.5 m^2 collection area, and the collection periods of each individual sample cup were programmed depending on the expected time of ice cover and/or the seasonality of the production. The sampling cups were filled with filtered sea water enriched in sodium chloride (NaCl) to achieve a salinity of 40 psu, and they were poisoned with mercury chloride (HgCl$_2$; 0.14 % final solution) for sample preservation. For FEVI16 samples,

5 zooplankton 'large swimmers' were removed using forceps before splitting each sampling cup into smaller sub-samples (Lalande et al., 2016). For PF3 samples, large swimmers were removed using forceps and a sieve (mesh size: 1 mm mesh) in the laboratory (Fischer et al., 2002). Afterwards, the samples were split for different purposes. A current meter (RCM 9/11) was attached to both trap moorings, and the data sets are available on PANGAEA (https://doi.org/10.1594/PANGAEA.845610; FEVI16) and in Walter et al., (2001; PF3)

10 **3.2 Mass flux**

Split FEVI16 samples were filtered onto GF/F filters (pre-combusted at 500 °C for 4 h) for organic carbon, organic nitrogen (PON), and carbonate, and onto cellulose acetate filters for biogenic opal quantification. Organic carbon (POC) and organic nitrogen (PON) were measured with a CHN elemental analyzer after 0.1 N HCl treatment. Carbonate was calculated by subtracting the weight from total mass after 0.1 N HCl treatments and re-corrected according to the aragonite contents. The

15 detailed methods used for biogenic silica can be found in Lalande et al., (2016). Split PF3 samples were freeze-dried for further processing. Decalcified samples (6 N HCl) were analysed for POC using a CHN elemental analyzer. Total nitrogen (TN) was also determined. Carbonate was calculated by subtracting POC from total carbon (TC), which was directly measured without decalcification (carbonate = 8.33 × (TC - POC)). The methodology for the quantification of biogenic silica is described in Fischer et al., (2002).

20 **3.3 GDGT analyses**

For GDGT analysis, total lipids were extracted with a solvent mixture (9:1 v/v dichloromethane (DCM): methanol (MeOH)) using an ultrasonic bath for 10 min and a centrifuge for 5 min, after which the supernatant was decanted. This process was repeated three times and the supernatants were combined. Before the extraction process, a known amount of C$_{46}$-GDGT (internal standard) was added to each sample for GDGT quantification.

25 Following saponification of total lipids with 1 mL of 0.1 M potassium hydroxide (KOH) in a mixture of MeOH: purified water 9:1 (v/v) at 80 °C for two hours, neutral lipids (NLs) were recovered with 1 mL hexane (3 times). NLs were separated into F1 (apolar), F2 (ketone), and F3 (polar) polarity fractions eluted in 2 mL hexane, 4 mL DCM: hexane (2:1 v/v), and 4 mL DCM: MeOH (1:1 v/v), respectively, using deactivated silica-gel chromatography (mesh size: 70-230 µm).

The F3 polar fraction containing GDGTs was re-dissolved in 500 µL hexane: isopropanol 99:1 (v/v) and filtered through a

30 polytetrafluoroethylene (PTFE) filter (pore-size: 0.45 µm) into a glass insert of a 2 mL vial according to Hopmans et al., (2000). The filtered polar fraction was diluted with hexane: isopropanol 99:1 (v/v) to a concentration of approximately 2 mg/mL before the instrumental analysis.

GDGTs were analyzed using high-performance liquid chromatography/atmospheric pressure chemical ionization-mass spectrometry (HPLC/APCI-MS) according to Chen et al., (2014). Molecular ions *m/z* 1302, 1300, 1298, 1296, 1292 for isoprenoid GDGTs and 1050, 1036 and 1022 for branched GDGTs were determined and quantified in relation to the molecular ion *m/z* 744 of the C_{46}-GDGT. The late eluting peaks of OH-GDGT−0, −1, and −2 with *m/z* 1318, 1316, and 1314 were also determined in the *m/z* 1300, 1298, and 1296 scan, as described by Fietz et al., (2013).

A lab-internal standard sediment was repeatedly analysed along with the samples to assess the analytical error. The standard deviation of replicate analyses was 0.1 units of TEX_{86}^L and 6% for isoprenoid GDGT concentrations.

3.4 GDGT flux and indices

TEX_{86}^L values were calculated according to Kim et al., (2010).

$$TEX_{86}^L = Log_{10} \frac{[GDGT-2]}{[GDGT-1]+[GDGT-2]+[GDGT-2]} \tag{1}$$

where the numbers represent the number of cyclopentane moieties in the isoprenoid GDGTs.

TEX_{86}^L values were converted into temperatures using the following equation (Kim et al., 2010):

$$SST(°C) = 67.5 \times TEX_{86}^L + 46.9 \quad \left(R^2 = 0.86, \ n=396, \ calibration \ error: \pm 4°C\right) \tag{2}$$

GDGT flux represents the sum of fluxes of individual GDGTs, which are used for calculating TEX_{86}^L.

$$GDGT \ flux = [GDGT-1]+[GDGT-2]+[GDGT-3] \tag{3}$$

OH-GDGT based indices and estimated temperatures were calculated using the following equations (Eq.4 by Fietz et al., 2013; Eq. 5 and 6 by Lü et al., 2015):

$$\frac{[OH-GDGT-0]}{[Cren]} = 0.25 - 0.025 \times SST(°C) \ (R^2 = 0.58, \ n=13, \ calibration \ error: \pm 1.5°C) \tag{4}$$

$$RI-OH' = \frac{[OH-GDGT-1] + 2 \times [OH-GDGT-2]}{[OH-GDGT-0]+[OH-GDGT-1]+[OH-GDGT-2]} \tag{5}$$

$$RI-OH' = 0.0382 \times SST \ (°C) + 0.1 \ (R^2 = 0.75, \ n=107, \ calibration \ error: \pm 6°C) \tag{6}$$

BIT, an index of relative contribution of terrestrial versus marine input, was calculated according to Hopmans et al., (2004).

$$BIT = \frac{[I+II+III]}{[I+II+III+Cren]} \tag{7}$$

The Roman numerals I, II, and III refer to the branched GDGTs with 4, 5, and 6 methyl moieties, and Cren represents Crenarchaeol containing 4 cyclopentane moieties and 1 cyclohexane ring (Fig. 1). A terrestrial effect on TEX_{86} can be significant when the BIT value is >0.3 (Weijers et al., 2006).

5 MI, the methane index indicating the relative contribution of GDGTs derived from methanotrophic Archaea to those from planktonic Thaumarchaeota was calculated as follows (Zhang et al., 2011):

$$MI = \frac{[GDGT-1]+[GDGT-2]+[GDGT-3]}{[GDGT-1]+[GDGT-2]+[GDGT-3]+[Cren]+[Cren']} \tag{8}$$

Cren´ represents the regio-isomer of Crenarchaeol. Contributions from methanotrophic Archaea are considered to be significant when MI>3.

10 %GDGT-0, an indicator of a methanogenic source of GDGTs with a %GDGT value >67 %, was calculated as follows (Inglis et al., 2015):

$$\%GDGT-0 = \frac{[GDGT-0]}{[GDGT-0]+[Cren]} \times 100\% \tag{9}$$

RI, the ring index, is a tool for identifying a potential non-thermal influence on GDGT distributions. A sample´s ring index is defined as follows (Zhang et al., 2016):

15 $$RI_{sanple} = 0 \times [GDGT-0]+1 \times [GDGT-1]+2 \times [GDGT-2]+3 \times [GDGT-3]+4 \times [Cren]+4 \times [Cren'] \tag{10}$$

$\lvert \Delta RI \rvert$ indicates the residual of a sample´s RI (RI_{sample}) from a calculated RI ($RI_{calculated}$) based on the global TEX_{86}−RI regression. $RI_{calculated}$ and $\lvert \Delta RI \rvert$ are defined as follows:

$$RI_{calculated} = -0.77(\pm 0.38) \times TEX_{86} + 3.32(\pm 0.34) \times (TEX_{86})^2 + 1.59(\pm 0.10) \ (R^2 = 0.87, n = 531) \tag{11}$$

$$\lvert \Delta RI \rvert = RI_{calculated} - RI_{sample} \tag{12}$$

20 Potential non-thermal influences on TEX_{86} can be recognized when $\lvert \Delta RI \rvert$ is >0.3 (Zhang et al., 2016).

3.5 Environmental parameters

TEX_{86}^{L}-derived temperatures were compared to satellite-derived SSTs obtained by Advanced Very High Resolution Radiometer (AVHRR), which has a spatial grid resolution of 0.25° and temporal resolution of 1 day (Reynolds et al., 2007).

The satellite-derived SSTs were averaged over the collection period of each sample cup. The depth profiles of mean annual water temperature and nitrate concentration were obtained from the World Ocean Atlas 2013 (WOA13) representing averaged values for the years 1955-2012 (Garcia et al., 2013; Locarnini et al., 2013).

4   Results

4.1   Eastern Fram Strait: FEVI16

4.1.1 Mass and GDGT fluxes

The mass flux data of the FEVI16 trap have been published previously by Lalande et al., (2016). In summary, the mass flux (opal + POC + PON + lithogenic fluxes) measured at 1296 m water depth varied in between $18.5-652.9$ mg m^{-2} d^{-1}, with minima in the winter season (November 2007−February 2008; Fig. 3a). Lithogenic flux is presented separately in Fig. 3a due to its significantly higher contribution to total mass flux. The composition of sinking particles changed between seasons. Lithogenic material flux showed sudden pulses in spring (March and April−May 2008). POC was predominant in mid-July 2007. Carbonate flux was elevated in March, early-May and mid-June 2008. Opal was dominant in early-September 2007 and mid-May to June 2008.

GDGT fluxes varied between $7.2-85.9$ ng m^{-2} d^{-1} (Fig. 3b). Peaks of GDGT flux occurred in August−September 2007 and March, May−June 2008, while minima were observed in the winter season (November 2007−February 2008). The GDGT flux was strongly correlated with opal flux ($R^2 = 0.82$, $p<0.0001$) when two GDGT maxima in late-September 2007 and March 2008 were excluded, and with carbonate flux ($R^2 = 0.86$, $p<0.0001$) except for the last two months in May-June 2008 (Fig. 3a and b).

4.1.2 TEX$_{86}^{L}$ thermometry

TEX$_{86}^{L}$ values varied between $-0.70-0.64$ and their TEX$_{86}^{L}$-derived temperatures (Kim et al (2010) calibration) ranged between $0.6-3.7$ °C (Fig. 3b and f). The flux-weighted mean TEX$_{86}^{L}$ temperature during the trap deployment period was 2.8 °C. Two surface sediment TEX$_{86}^{L}$ values (-0.66 at PS68-251/2 (79.1° N, 4.6° E) and -0.65 at PS68-271/2 (79.3° N, 4.3° E)) are available near the FEVI16 trap (Ho et al., 2014). Most index values of BIT, MI, %GDGT-0, and │ΔRI│ for samples from FEVI16 were below the critical values of each index (>0.3 for BIT and MI, >67 % for %GDGT-0, >0.3 for │ΔRI│). One sample with a │ΔRI│ value >0.3 was found, indicating a non-thermal effect on TEX$_{86}$ (Table A1).

4.1.3 Fractional abundance of OH-GDGTs

All OH-GDGTs were clearly present in FEVI16 samples. OH-GDGT-0 was predominant in the OH-GDGT pool, accounting for 87−95 % (Fig. 4a). The proportion of OH-GDGTs in the sum of iso- and OH-GDGTs ranged between 7 and 11 % during the trap deployment period (Fig. 4a). Estimated temperatures calculated using the calibrations as described in Eq. (4) and (6)

(Fietz et al., 2013 and Lü et al., 2015) ranged between -0.3−2.5 °C and between -0.9−1.4 °C, respectively. The last two data points for the trap time series were unusually low when using Eq. (4) (Fig. 4b).

4.2 Antarctic Polar Front: PF3

4.2.1 Mass and GDGT fluxes

5   The mass flux data of the PF3 trap have been published previously by Fischer et al., (2002). The mass flux at the shallow trap ranged between 19.7−592.1 mg m^{-2} d^{-1} with a distinct seasonal variability (Fig. 5a). Flux maxima occurred in November 1989 to early-March 1990 and mid-October to November 1990, while it stayed relatively low from mid-March to mid-October 1990. At the deep trap, the mass flux varied between 0−516.6 mg m^{-2} d^{-1} (Fig. 5d). The mass flux peaked in mid-December 1989−January and March 1990 but stayed low for the remaining sampling period except for mid-May 1990.

10   There was no clear correlation between organic material and GDGT fluxes at neither depth. The fluxes in GDGTs ranged from 10.5 to 73.9 ng m^{-2} d^{-1} at 614 m and from 0.5 to 153.9 ng m^{-2} d^{-1} at 3196 m depth (Fig. 5b and e). GDGT fluxes were mostly enhanced during the low mass flux season at the shallow trap (Fig. 5b). GDGT flux maxima occurred in November and December 1989, late-May and early-November 1990 at the deep trap (Fig. 5e). GDGT analysis was not possible between late-July and October 1990 in the deep trap, since very little material was collected during this time period.

15   ### 4.2.2 TEX$_{86}^{L}$ thermometry

TEX$_{86}^{L}$ values varied between -0.58−0.67, and -0.55−0.59 at the shallow and deep trap, respectively (Fig. 5b and e). The TEX$_{86}^{L}$-derived temperatures ranged between 1.3−7.8 °C for the shallow trap, and 7.4−9.8 °C for the deep trap (Fig. 5c and f). The flux-weighted mean TEX$_{86}^{L}$ temperatures were 4.6 °C and 8.5 °C at the shallow and deep traps, respectively. In some samples, GDGT-3 was below the detection limit. In these cases, TEX$_{86}^{L}$ values and estimated temperatures were not included

20 on the figures, but GDGT flux was calculated. A surface sediment TEX$_{86}^{L}$ value of -0.56 (CHN-115-4-34; 51.00° S, 5.33° E) in the vicinity of the PF3 trap site (50.13° S, 5.83° E) can be found in the TEX$_{86}$ global calibration dataset (Kim et al., 2010), and its TEX$_{86}^{L}$-derived temperature estimate is 9.1 °C. Most samples did not exceed the index values indicating non-thermal impacts on TEX$_{86}$ (see Sec. 3.4). Two samples from the deep trap between early November and late December 1989, however, showed MI values between 0.3 and 0.5 (Table A1).

25   ### 4.2.3 Fractional abundance of OH-GDGTs

All OH-GDGTs were clearly present in samples from both depths. OH-GDGT−0 was predominant in the OH-GDGT pool (76−89 % for the shallow trap, 77−83 % for the deep trap; Fig. 6a and c). The proportion of OH-GDGTs in the sum of iso- and OH-GDGTs ranged from 4−7 % and 5−6 % at the shallow and deep trap, respectively, (Fig. 6a and c). Estimated temperatures calculated according to Eq. (4) and (6) ranged between 3.0−6.1 °C and 1.1−5.1 °C in the shallow trap (Fig. 6b).

30 With the same calibrations, estimated temperatures varied between 3.6−5.8 °C and 2.8−5.2 °C in the deep trap (Fig. 6d).

5 Discussion

5.1 Eastern Fram Strait (79° N)

5.1.1 GDGT flux and particle export

Organic matter (including GDGTs), formed in the upper ocean, is exported to the bathypelagic mainly as zooplankton fecal pellets or marine snow aggregates (Fischer and Karakaş, 2009; Wuchter et al., 2006b). The velocities of the sinking aggregates vary depending on their composition (Fischer and Karakaş, 2009; Iversen and Ploug, 2010) and physical characteristics. For instance, aggregates formed from coccolithophores are ballasted by carbonate and may sink faster than opal ballasted diatom aggregates (Iversen and Ploug, 2010). Still, fecal pellets formed from either coccolithophores or diatoms sink faster than fecal pellets formed from non-ballasted flagellates (Ploug et al., 2008a, 2008b). GDGTs have been suggested to be preferentially incorporated into opal-dominated particles (Mollenhauer et al., 2015). This is in agreement with observed TEX_{86}-derived temperatures in sediment-trap samples off Cape Blanc being delayed relative to the SST signal, and this time delay was longer than for $U_{37}^{K'}$-derived temperatures (Mollenhauer et al., 2015).

GDGT fluxes co-varied with fluxes of biogenic- and non-biogenic components in the eastern Fram Strait (Fig. 3). GDGT fluxes were enhanced in summer 2007 and spring 2008 with two clear maxima in late September 2007 and March 2008 (Fig. 3b). Without those two distinct GDGT flux maxima, GDGT flux showed a good correlation with opal ($R^2 = 0.82$, $p<0.0001$) throughout the deployment period. Those two episodic GDGT pulses occurred when carbonate, coccolithophore, and terrestrial biomarker fluxes were enhanced, potentially resulting in the enhanced GDGT flux (Chen et al., 2016; Yamamoto et al., 2012). GDGT fluxes co-varied also with carbonate from the beginning of the deployment until April 2008 ($R^2 = 0.8$, $p<0.0001$) (Fig. 3a and b). This agrees with the concept that GDGTs are transported by particles mainly containing opal and carbonate as previously shown in sediment trap studies (Chen et al., 2016; Huguet et al., 2007; Mollenhauer et al., 2015; Park et al., 2018; Yamamoto et al., 2012). This observation suggests that GDGTs are exported together with diatoms (opal) and coccolithophores (carbonate). Supporting this, diatom and coccolithophore fluxes both, previously reported by Lalande et al., (2016), showed good correlations with GDGT fluxes ($R^2 = 0.64$, $p<0.001$ for diatoms and $R^2 = 0.68$, $p<0.0001$ for coccolithophores) when excluding two GDGT flux maxima in the correlations with opal fluxes. The flux of terrestrial biomarkers (campesterol+ß-sitosterol), previously analyzed by Lalande et al., (2016), also showed a positive correlation with GDGT flux ($R^2 = 0.64$, $p<0.001$). The sterols (campesterol and ß-sitosterol), used frequently to assess the plant-derived organic matter input to aquatic systems (Moreau et al., 2002), reflect the input of terrestrial matter transported by sea-ice in the Fram Strait (Lalande et al., 2016). We thus assume that terrestrial material is aggregated into particles which carry GDGTs. However, the lithogenic flux, also representing terrestrial input, displayed a different trend with maxima only in mid-April−mid-May 2008, when the sea ice concentration abruptly increased (Fig. 3e). The lithogenic material seems to be mainly supplied by downslope export from the nearby Svalbard archipelago (Lalande et al., 2016), with a significant input when the sea ice is present (Fig. 3e).

GDGTs might also be exported with fecal pellets after grazing of Archaea by zooplankton. Indeed, GDGTs have been found in decapod guts and intestines, and their abundance ratios appear to be unaltered during gut passage (Huguet et al., 2006). The fecal pellet carbon (FPC) flux from appendicularians contributed more to the total carbon flux than copepod FPC flux. Both appendicularian and copepod FPC fluxes were higher during spring 2008 than during summer 2007 (Fig. 3d; Lalande et al., (2016)). The correlation of GDGT fluxes with appendicularian FPC fluxes ($R^2 = 0.67$, $p<0.05$ in mid-July to mid-October 2007) implies grazing of Archaea by the appendicularians. Appendicularians are well known to ingest micro-size particles like Archaea (<1 µm) efficiently through a fine mucus filter (Conley and Sutherland, 2017).

Overall, it is reasonable to assume that seasonal changes in the relative proportion of materials that GDGTs can be aggregated with, may result in variable export velocities of particles carrying GDGTs to deeper waters in the eastern Fram Strait.

5.1.2 Variability of TEX_{86}^L-derived temperature

TEX_{86}^L temperatures varied (-0.2−3.7 °C) within a similar range as the satellite-derived SSTs (-0.1−3.4 °C) during the trap deployment period in the eastern Fram Strait. Although it did not display a clear seasonality, the TEX_{86}^L signal is most likely to reflect the surface water environments without non-thermal effects influencing the TEX_{86}^L (Fig. 3e). First of all, when the error the TEX_{86}^L calibration (±4 °C) is considered, the SST estimates are identical to the satellite-derived SSTs. Secondly, the index values (e.g. BIT, MI, %GDGT-0, RI), which could indicate potential non-thermal factors influencing the distribution of GDGTs, suggest that TEX_{86}^L temperatures should reflect the upper water column temperature (Table A1). The BIT index defined by Hopmans et al., (2004) as a tracer for the terrestrial organic matter input was very low (<0.02), showing that negligible amounts of soil-derived GDGTs are entrained in sinking particles. MI (Zhang et al., 2011) and %GDGT-0 (Inglis et al., 2015) have been suggested as indicators for the impact of methanotrophic Archaea even though it was questioned if the latter index can be applied in marine settings (Inglis et al., 2015). Both index values were consistently lower than the respective critical values of 0.3 for MI and 67 % for %GDGT-0. │ΔRI│ was suggested by Zhang et al., (2016) as an indicator for the integrated non-thermal factors on TEX_{86}. Most │ΔRI│ values were lower than a value of 0.3, and only three samples collected in late September 2007 and June 2008 satisfied the criteria of being influenced by non-thermal factors. Lastly, although significant portions of particles transported to the mid-depth and deep water in the eastern Fram Strait originated off Svalbard and the Barents Sea (Lalande et al., 2016), it is known that GDGTs are most likely to reflect the local conditions rather than being affected by lateral transport (Kim et al., 2009; Mollenhauer et al., 2008). Therefore, we conclude that GDGTs are mainly transported from upper waters and non-regional sources of particles do not play a significant role for the TEX_{86}^L estimate in sinking particles of the eastern Fram Strait.

TEX_{86}^L temperatures varied strongly between mid-July−October 2007, with the minimum estimated temperature (0.6 °C) when the GDGT and terrestrial biomarker fluxes were highest (Fig. 3b, c, and f). This is the most productive period in the Fram Strait and also the period with the highest export fluxes (e.g. Lalande et al., 2016). The material collected by deep

ocean sediment traps is a mixture of many types of aggregates with different composition and settling velocities. Therefore, fluctuating TEX_{86}^L temperatures might be due to an average of signals from previous (before mid-July, i.e. slowly sinking particles) and current seasons (mid-July to October, i.e. fast settling aggregates), which were exported via different aggregation and sinking mechanisms with different horizontal displacements during particle descent. Due to the collection of aggregates sinking with different velocities, one sample cup in a sediment trap may collect GDGTs of different ages.

During the low flux period between November 2007−February 2008, TEX_{86}^L temperatures were constantly lower than the satellite-derived SSTs (Fig. 3a, b, and f). These signals might be derived from GDGTs synthesized in mid-August to October, which was a late-bloom period dominated by protists that do not produce biominerals, such as *Phaeocystis* sp., dinoflagellates, and nanoflagellates (Nöthig et al., 2015). Aggregates formed without biominerals have low sinking velocities (Iversen and Ploug, 2010; Ploug et al., 2008a, 2008b), which may explain why the satellite-derived SSTs from mid-August to October 2007 were similar to the TEX_{86}^L-derived temperatures in sinking particles collected during November 2007 and February 2008. In spring 2008, TEX_{86}^L temperatures stayed relatively warm until mid-April and suddenly dropped in May and June (Fig. 3f). The relatively warm TEX_{86}^L temperatures in particles collected in March and April 2008 probably reflect the signal transported by GDGTs produced in November−December 2007. Warm and cold biases of the TEX_{86}^L-derived temperatures varied within the calibration error (±4 ℃) throughout the trap deployment period. It shows that the bias of the calibration occurs neither in one direction only nor to the same extent even at a given location, instead the temperature estimate is more affected by other processes discussed above. Like previous seasons, the lack of transporting materials for GDGTs delayed the TEX_{86}^L signal. The sudden drop of TEX_{86}^L-derived temperatures in mid-May to June 2008 was matched with the season of the enhanced flux of biogenic materials, GDGTs, phytoplankton, zooplankton fecal pellets and terrestrial biomarkers at the trap when the sea ice concentration was enhanced (Fig. 3). Eddies around the ice-edge create upwelling and downwelling, which breaks the stratified surface water and supplies nutrients to the upper water column, fostering phytoplankton blooms (Lalande et al., 2013). The sea ice-edge bloom probably enhanced the GDGT production followed by zooplankton grazing. Additionally, the terrestrial materials as ballast were more available, which were derived from sea-ice as it melted during spring 2008. This process caused the fast export of TEX_{86}^L signal from the surface waters in mid-May to June 2008. Overall, the particles containing GDGTs captured at 1296 m depth in the eastern Fram Strait were likely delivered by a combination of packaging mechanisms involving biological and non-biological transport materials with different delay times over the season. Moreover, most GDGTs are exported vertically from the upper waters and reflect a regional TEX_{86}^L signal in the eastern Fram Strait (Figure 3f), while significant particle supply from the south via lateral advection has been reported previously (Lalande et al., 2016). The reflection of SSTs based on the TEX_{86}^L calibration and the good correlation of GDGTs with opal and Appendicularian fecal pellet fluxes agrees with the finding that diatom and fecal pellet fluxes can be traced as the export of local production regardless of the lateral particle supply in the Fram Strait (Lalande et al., 2016).

The average export velocity of particles containing GDGTs can be calculated by dividing the travel distance of particles (i.e., the depth of the sediment trap) by the temporal offset between TEX_{86}^L-derived temperature and the corresponding satellite-derived SST, greatly simplifying the complexity of sinking mechanisms and range of settling velocities throughout the season (Mollenhauer et al., 2015). When the TEX_{86}^L-derived temperatures are shifted by 82 days, we found the best fit to the

5   satellite-derived SSTs (Fig. 7b). Therefore, we see that GDGTs synthesized in the eastern Fram Strait likely travel to the trap (1296 m) approximately within 82 days. This translates into an average minimum export velocity of GDGT-containing particles of approximately 15 m d^{-1} when assuming export from 30-80 m water depth (see below Sec. 5.1.3). We have assumed that the export velocity includes the time of GDGT synthesis and transport time to the trap. The estimated sinking velocity of 15 m d^{-1} is within range (9−17 m d^{-1}) estimated at a similar water depth (~1300 m) in the filamentous upwelling

10 zone off northwest Africa (Mollenhauer et al., 2015) and only slightly lower than settling velocities found previously for aggregates from the Fram Strait (Wekerle et al., 2018). Based on the seasonal succession of peaks in appendicularian fecal pellets in the same mooring system, their sinking velocity was estimated to be 5- to 11- fold higher (15−35 days to 2400 m depth; Lalande et al., 2016) compared to GDGTs. This is a realistic scenario because of the fast sinking velocity of a fecal pellet, being rather big and dense, and generally faster average export velocities to deeper ocean depths (Fischer and Karakaş,

15 2009; Iversen et al., 2017). Moreover, the average export velocity of GDGTs includes the time it takes to be incorporated into aggregates. A more rapid export of GDGTs to depth resulting in smaller temporal offsets of TEX_{86}^L-derived temperature to water temperature changes occurred in mid-May−June 2008 when the FPC flux of appendicularians was enhanced (Fig. 3d). It has to be noted that the export velocity we calculated here may represent an averaged velocity of all the aggregates collected in the trap, as the export velocity of GDGTs can vary depending on the type of sinking materials GDGTs are

20 incorporated into.

   The flux-weighted mean TEX_{86}^L temperature over the mooring period was 2.8 °C. In the vicinity of the site FEVI16 (79.03° N, 4.35° E), two TEX_{86}^L values from surface sediments are available in the dataset published by Ho et al., (2014). The estimated temperatures based on TEX_{86}^L are 2.8 °C and 2.3 °C in PS68-251/2 (79.30° N, 4.30° E) and PS68-271/2 (79.10° N, 4.60° E), respectively. Considering the error of the TEX_{86}^L calibration (Kim et al., 2010), TEX_{86}^L estimates are almost

25 identical between sinking particles and surface sediments. This suggests that GDGTs synthesized in the upper waters are propagated through the water column into the sediment without significant alteration even though the sinking process of GDGTs in the eastern Fram Strait seems quite complicated as discussed above. Iversen et al., (2010) and Jackson and Checkley Jr. (2011) also suggested that most biological activities resulting in aggregate alteration and degradation occur around the base of the photic zone. Our observations agree with previous studies, as TEX_{86} displays consistent values at

30 multiple depths and/or in the underlying surface sediments in various environmental regimes such as in the Arabian sea (Wuchter et al., 2006b), in the northwestern Pacific (Yamamoto et al., 2012), off Cape Blanc (Mollenhauer et al., 2015), near Iceland (Rodrigo-Gámiz et al., 2015), off southern Java (Chen et al., 2016), and in the northern Gulf of Mexico (Richey and Tierney, 2016).

In the eastern Fram Strait, the changes of TEX_{86}^L-derived temperature are largely controlled by the depth and time of GDGT production and temporally variable sinking materials aggregated with GDGTs. Additionally, the absolute estimated temperatures varied within the TEX_{86}^L calibration error (±4 ℃). In this case, the temperature error inherited from the calibration is less important than other relative changes.

5 **5.1.3 Potential depth of TEX_{86}^L signal origin**

To determine the water depth where the TEX_{86}^L signal originated, the flux-weighted mean TEX_{86}^L temperature (2.8 ℃) was compared to the depth profile of nutrient concentrations (NH_4^+, NO_2^-, and NO_3^-) measured in late June to early July 2010, 2011, and 2013, and water temperature extracted from WOA13 (79.125° N, 4.375° E) in the eastern Fram Strait (Fig. 8). Unfortunately, ammonia data are unavailable in 2007 and 2008. The mean estimated temperature (2.8 ℃) in sinking

10 particles corresponds to the surface water in July−September or of 30−80 m subsurface waters in April−June (Fig. 8). Major production of GDGTs in both seasons is a possible scenario because GDGT flux peaked in both seasons (Fig. 3b). However, the latter period (April−June) is the more plausible season dominantly supplying GDGTs to the sediment if we consider the delay time of the GDGT signal (approximately 82 days, see Sec. 5.1.2), which illustrates the initial time of GDGT production (Fig. 3b). Furthermore, Thaumarchaeota, the primary synthesizers of GDGTs in the ocean, are aerobic ammonia

15 oxidizers (Könneke et al., 2005) and maximum GDGT concentrations have been found near the NO_2^- maximum, where maximum rates of ammonia oxidation and nitrification occur (Beman et al., 2008; Hurley et al., 2016). The depths of consumption of ammonia and production of nitrite as well as nitrate accumulation as a result of the nitrification process in the subsurface can be deduced from the nutrient profile (Fig. 8). Assuming that maximum thaumarchaeotal abundance occurs at the depth of highest substrate availability, we, therefore, infer that Thaumarchaeota mainly record the subsurface

20 water temperature (30−80 m) during the warm season when the spring bloom may occur (April−June) in the eastern Fram Strait. Similar observations were made in the Sea of Okhotsk and the north-west Pacific (Seki et al., 2014) and in the western Bering Sea (Meyer et al., 2016), where the TEX_{86}^L-derived temperature is attributable to the regional season and water depth of GDGT production. The temperatures measured by a temperature sensor attached to the mooring array at approximately 68 m depth (Beszczynska-Möller et al., 2012a), which is approximately in the middle of the depth interval (30−80 m)

25 corresponded to the TEX_{86}^L temperature (Fig. 8), support our interpretation. The flux-weighted mean TEX_{86}^L temperature is well within the range of measured temperatures at this depth and it reflects well the temperatures in March−June as deduced from the nutrient depth profile (Fig. 7c).

5.2 Antarctic Polar Front (50° S)

5.2.1 GDGT flux

30 At the shallow trap (614 m water depth) of site PF3, there was no clear correlation between fluxes of organic matter and GDGTs, which displayed their respective maxima in different seasons (Fig. 5a and b). Peaks of mass flux occurred in

November 1989−early-March 1990 and mid-October−December 1990, while GDGT fluxes were highest in mid-May−June and late July−August 1990 (late austral autumn and winter) (Fig. 5a and b). Similar observations were made in the North Sea, where the abundance of Thaumarchaeota (previously known as marine group I Crenarchaeota) and GDGT concentrations were high in winter time, supported by the seasonality of Thaumarchaeotal 16S rRNA and amoA gene abundances in that

5   region (Herfort et al., 2007; Pitcher et al., 2011; Wuchter et al., 2006a). An austral "winter bloom" of planktonic Archaea was also found near the Antarctic Peninsula (Church et al., 2003; Murray et al., 1999; Tolar et al., 2016). Photoautotrophic phytoplankton, which use ammonium as a N source, would outcompete Archaea for ammonia in spring and summer time. In contrast, in winter time when phytoplankton productivity is limited due to the lack of light, ammonia availability for Archaea is higher (Pitcher et al., 2011; Wuchter et al., 2006b). This explains the winter bloom of ammonia-oxidizing Archaea. Laubscher et al., (1993) found that

10   ammonia was highly depleted at the chlorophyll-a maximum across the Antarctic Polar Front in early austral summer, which might create less favorable conditions for ammonia-oxidizing planktonic Archaea. Additionally, Thaumarchaeota are known to be sensitive to photoinhibition (Horak et al., 2017). Therefore, the austral winter maxima in GDGT flux at the shallow trap of PF3 might be a consequence of the higher production of planktonic Archaea in surface waters of the APF during the time when ammonia is more available and photoautotrophs cannot compete due to light limitation.

15   At the deep trap (3196 m water depth) of site PF3, GDGT flux peaked in November 1989 while mass flux was most pronounced in March 1990 (Fig. 5d and e). Due to the lack of sinking particles captured in the deep trap in June−November 1990, it is unclear if a potential "winter bloom" of GDGTs was also exported to deeper waters. The trapping efficiency of PF3 was found to be below 50 % at the deep trap using ^{230}Th as flux proxy (Walter et al., 2001). The negligible mass flux could thus be caused by low trapping efficiency. However, Fischer et al., (2002) observed a similar seasonal flux pattern in the

20   following years measured almost at the same depths and at the same location as site PF3. At site BO (54.50° S, 3.33° W), which was located further south than site PF3, the authors also found a period of almost no flux in July-December for four years approximately at 2200 m depth. Thus, it is assumed that a low trapping efficiency or a failure of the trap system did not account for the lack of particle samples at the deep trap of PF3.

5.2.2 Variability of TEX_{86}^{L}-derived temperature

25   TEX_{86}^{L}-derived temperatures at the shallow trap did not display a clear seasonal variability. Only 1/3 of the data points were similar to the SSTs, while the remaining samples showed warm or cold biased temperatures relative to the satellite-derived SSTs during the sampling period (Fig. 5c). All samples in the deep trap displayed warmer TEX_{86}^{L} temperatures by up to 7 °C relative to the satellite-derived SSTs (Fig. 5f). As discussed above, the mismatch between lipid proxy-based temperature estimates and satellite-derived temperature could be explained by the delay time of the proxy signal, due to the time needed

30   between lipid synthesis and incorporation into sinking aggregates plus the sinking time (Mollenhauer et al., 2015; Müller and Fischer, 2003; Park et al., 2018). However, without a marked seasonality of the estimated temperature, it is difficult to determine a delay time of the TEX_{86} signal. The other explanation for the absence of covariance between the TEX_{86} signal

and the satellite-derived SST is that we observe a mixed signal of Thaumarchaeotal GDGTs derived from surface and deep ocean. The warm biases have a tendency to occur during periods of lower GDGT flux and thus may include higher proportions of material from different sources (early-December, mid-June−July, September−November), which may be more dominant in the deep trap (see discussion below).

5   Temperature residuals (~7 ℃) in the deep trap, which are larger than the calibration error (±4 ℃), suggest significant non-thermal effects on GDGT compositions or the unreliability of the global calibration in this region.

Warm-biased TEX_{86}^{L}-derived temperatures have been attributed to the contribution of different archaeal communities or GDGT input from terrestrial sources, which may alter the composition of pelagic GDGTs, leading to unusual TEX_{86}^{L}-derived temperature estimates (Hopmans et al., 2004; Inglis et al., 2015; Zhang et al., 2011, 2016). For example, several studies

10   showed that anomalous TEX_{86} based temperature estimates can be caused by isoprenoid GDGTs produced by Group II Euryarchaeota as significant contributors to the archaeal tetraether lipid pool and, thus, TEX_{86} (Lincoln et al., 2014; Schouten et al., 2008, 2014; Turich et al., 2007), a suggestion that is controversial. A prevalence of marine Group II Euryarchaeota has been reported in Circumpolar Deep Waters (Alonso-Sáez et al., 2011) and in deep waters of the Antarctic Polar Front (López-García et al., 2001; Martin-Cuadrado et al., 2008; Moreira et al., 2004; Murray et al., 1999). Therefore,

15   we would assume that GDGTs produced by deep-dwelling Euryarchaeota might have caused the warm-biased TEX_{86}^{L} signal at depth in the region. Alternatively, advection of particles from warmer ocean regions could potentially lead to warm biases. However, it is known that the impact of lateral transport of GDGTs on the local signal is insignificant (Kim et al., 2009; Mollenhauer et al., 2008).

BIT, MI, %GDGT-0, and │ΔRI│ were examined to evaluate non-thermal factors on GDGT composition and TEX_{86} values

20   at both PF3 traps. However, none of the values for BIT, %GDGT-0, and │ΔRI│ exceeded the defined critical values (Table A1). MI values were higher at the deep trap than at the shallow one. The first two samples at the deep trap reached values of 0.3−0.5 MI, suggesting that GDGTs are derived from a mixture of non-methanotrophic and methanotrophic communities (Zhang et al., 2011). However, these two samples alone cannot fully explain the episodic and continuous warm-biased TEX_{86}^{L} estimates at the shallow and deep trap. Therefore, those indices cannot explain the warm anomaly of TEX_{86}^{L} estimates

25   in the APF. Like in the Gulf of Mexico (Richey and Tierney, 2016), a longer time series of samples would be helpful to investigate inter-annual variability, paired with a direct assessment of the archaeal community in the region.

The flux-weighted mean TEX_{86}^{L} temperatures averaged over the trap deployment period were 4.6 and 8.5 ℃ at the shallow and deep traps, respectively. The TEX_{86}^{L} temperature in surface sediment (CHN 115-4-34; 51.00° S, 5.33° E) from the vicinity of the PF3 trap was 9.1 ℃, which is 4.5 ℃ warmer than the TEX_{86}^{L} estimate temperature in the shallow trap (4.6 ℃)

30   but is similar to the one in the deep trap (8.5 ℃). This situation is different from the Fram Strait and other time-series trap studies which showed that TEX_{86} values in different depths are almost identical (Chen et al., 2016; Mollenhauer et al., 2015; Wuchter et al., 2006b). This implies that there is a clearly different origin of GDGTs in particles collected in the upper (<~ 600 m) and deeper ocean, yet the main explanation of the warm-biased TEX_{86}^{L} is still speculative.

5.3 Re-evaluation of TEX_{86}^L calibration in polar oceans

In the two previous sections, the TEX_{86}^L calibration developed by Kim et al., (2010) for regions where maSSTs are below 15 ℃ was applied. This calibration is based on data from 396 surface sediments in the global ocean. Several studies have expanded the TEX_{86} and TEX_{86}^L surface sediment dataset. We revisited the latest global surface sediment dataset containing 1095 surface sediment measurements (Tierney and Tingley, 2015 and reference therein) to recalculate the TEX_{86}^L calibration and to examine the agreement of our results with the new calibration. From the dataset, the data points for which TEX_{86}^L values cannot be calculated or which were pointed out as problematic by Ho et al., (2014) (c.f. BIT>0.3 or ~ 1.0 and GDGT concentration below detection limit) were excluded to avoid potential biases. With approximately two times more data points for the TEX_{86}^L calibration than the original one (Kim et al., 2010; n = 396), the new calibration again shows a linear correlation with maSSTs even though the correlation coefficient is slightly lower (Fig. 9; $TEX_{86}^L = 0.013 \times SST - 0.657$; R^2 = 0.80, n = 744) and the residual standard error (± 5.0 ℃) is higher than those of the Kim et al., (2010)'s calibration (R^2 = 0.86, ± 4.0 ℃). It should be noted that our new linear calibration has SST on the x-axis as the control variable and TEX_{86}^L value on the y-axis as the dependent variable because the composition of GDGTs, membrane lipids of Thaumarchaeota, (i.e., TEX_{86}/ TEX_{86}^L value) is affected by water temperature. This different regression might explain parts of the discrepancy between our and the original calibrations of Kim et al. (2010). Larger scatter towards colder temperatures appear in the new calibration as shown in previous studies (Ho et al., 2014; Kim et al., 2010) (Fig. 9).

It is obvious that the relationship of maSSTs and TEX_{86}^L values in high latitude northern (>50° N) and southern (>50° S) oceans is significantly different when both regions are plotted separately (Fig. 9). The data from the north (>50° N) are scattered both on the right- and left-hand side of the regression line, resulting in potential warm and cold anomalies, respectively (Fig. 9). This may reflect various sources of GDGTs in the high latitude northern oceans, which have direct geographical connections to Eurasia and North America. Warm biased TEX_{86}^L estimates in these regions might be caused by input of soil-derived GDGTs, which are picked up by the sea ice in the Arctic marginal seas (c.f. Laptev sea, Kara Sea, eastern Greenland), and released while the sea ice melts. Alternatively, TEX_{86}^L-derived temperatures might reflect warmer subsurface temperatures in the warm season as shown in the subarctic North Pacific region with the regional calibration by Seki et al., (2014) and Meyer et al., (2016). Cold-biased TEX_{86}^L estimates are mainly found in the Barents Sea, North Sea, and the Norwegian Sea. In the North Sea, a significantly enhanced abundance of planktonic Archaeal cells and high GDGT concentration in the winter time could account for colder TEX_{86}^L-derived temperature compared to SST (Herfort et al., 2007; Pitcher et al., 2011; Wuchter et al., 2006a). Hence, regional calibrations in the high latitude northern oceans seem to be a valid approach.

By contrast, most of the data from the south (>50° S) show higher TEX_{86}^L values than predicted by the regression line (n = 95). This explains the observed warm anomalies of TEX_{86}^L-derived temperature when using the original linear regression calibration. Instead of the global linear calibration, a polynomial one seems to be a better option in these regions (Fig. 9).

When excluding one data point in the winter sea ice-covered Southern Ocean, the correlation coefficient of the polynomial correlation is encouraging ($R^2 = 0.63$).

The data points of the flux-weighted mean TEX_{86}^L in the FEVI16 trap and TEX_{86}^L in the underlying surface sediment against maSSTs are both closely located to the linear regression line. It illustrates the applicability of the linear TEX_{86}^L calibration in

5   the eastern Fram Strait (Fig. 9). At the site PF3, the TEX_{86}^L-derived temperatures based on the polynomial calibration yield - 0.1 ℃, 1.9 ℃, and 2.2 ℃ at the shallow and deep trap, and in the underlying surface sediment, respectively (Fig. 9), which are colder than the estimates based on the linear calibration. The polynomial TEX_{86}^L temperatures at the deep trap and on the sediment are slightly colder than maSST (2.4 ℃, the data can be found in Tierney and Tingley, (2015)), but less biased compared to the reconstructed temperatures based on the linear TEX_{86}^L calibration (see Sec. 5.2.2). To test this polynomial

10   calibration in the southern ocean (>50 °S), a further assessment needs to be made with down-core sediments in similar regions, where the original TEX_{86}^L estimate displays a warm bias.

5.4   Applicability of OH-GDGT related calibrations for SST estimates in the high latitude Atlantic Ocean

OH-GDGTs were determined in sinking particles of the eastern Fram Strait and of the APF. The proportions of OH-GDGTs to total GDGTs (sum of OH- and iso-GDGTs) ranged between 7−14 % in the eastern Fram Strait and 4−7 % in the APF (Fig.

15   4a, 6a, and 6c). This is a relatively smaller portion than in the Nordic Seas (~ 16 %; Fietz et al., 2013).

Several OH-GDGT based calibrations for SST have been suggested for the global ocean and the Nordic Seas (Fietz et al., 2013; Huguet et al., 2013; Lü et al., 2015). We applied those calibrations suggested by Fietz et al., (2013) and Lü et al., (2015). Only two calibrations (Eq. 4 and 6) yield realistic temperature estimates, which varied within a similar range as satellite-derived SSTs or TEX_{86}^L-derived temperatures (Fig. 4b, 6b and 6d). The former calibration considers relative

20   abundances of OH-GDGT−0 and Crenarchaeol (Eq. 4). The latter is based on the RI-OH-GDGTs (Eq. 5 and 6). In the eastern Fram Strait, both OH-GDGTs based temperatures showed similar changes with an increasing trend until late-April 2008 and decreasing temperatures in May 2008 except for the last two samples (Fig. 4b). In the APF, both OH-GDGTs based temperatures were also close to the satellite-derived SSTs and the TEX_{86}^L-derived temperatures at the shallow trap (Fig. 6b). Warm biases as the TEX_{86}^L calibration did not occur with those OH-GDGTs calibrations at the deep trap (Fig. 6d). We

25   speculated in Sec. 5.2.2 that the warm-biased TEX_{86}^L temperatures relative to SSTs may be caused by GDGTs synthesized by Euryarchaeota dwelling in deep waters of the APF. The methanogenic Euryarchaeota are known to produce GDGT−1, −2 and −3 and may alter the TEX_{86} signal derived from pelagic Thaumarchaeota (Weijers et al., 2011). This might explain why only calibrations (OH-GDGT/Cren and RI-OH′), which do not contain GDGTs potentially originated from Euryarchaeota, show a correspondence to regional SSTs. At this stage, however, this has to be considered speculative. Moreover, it is not

30   clear yet if OH-GDGTs are exclusively produced by Thaumarchaeota since OH-GDGTs were also detected in a culture of Euryarchaeota (*Methanothermococcus thermolithotrophicus*) (Liu et al., 2012). Therefore, further research is needed to

clarify various aspects of distribution, production, and modification of OH-GDGTs in response to physicochemical changes in the global ocean. Nonetheless, OH-GDGTs appear to be a potential temperature proxy in our two high latitude regions.

6   Summary and Conclusions

Sinking particles collected using time-series sediment traps allowed us to determine the variability of the downward GDGT export and the environmental influence on TEX_{86}^L thermometry in northern and southern high latitude regions of the Atlantic Ocean. We observed fundamentally different patterns between the eastern Fram Strait and the Antarctic Polar Front (Table 2).

In the eastern Fram Strait, the seasonally different composition of sinking materials resulted in different sinking velocities of GDGTs, and thus the temporal offsets between TEX_{86}^L-derived temperatures and SSTs may vary by season. Although increased flux of terrestrial matter transported by sea-ice in intermediate and deep waters is well known in the region (Lalande et al., 2016), TEX_{86}^L thermometry does not seem to be affected by lateral advection of particles. The flux-weighted mean TEX_{86}^L temperature in sinking particles was similar to the one in the underlying surface sediment, indicating that the TEX_{86}^L signal did not experience substantial changes while sinking. The flux-weighted mean TEX_{86}^L temperature corresponded to temperatures in water depths ranging between 30 and 80 m, where nutrient profiles suggest favorable conditions for Thaumarchaeota.

In the Antarctic Polar Front, changes in GDGT fluxes and TEX_{86}^L temperatures are different between the two traps moored at different depths. At the shallow trap, TEX_{86}^L estimates do not co-vary with satellite-derived SSTs, and its flux-weighted mean temperature is 4.6 °C. The warm-biased TEX_{86}^L at the deep trap and in the underlying surface sediment may be caused by GDGT contributions from Euryarchaeota, which is dominant in the deeper part of the water column of CDW at the Antarctic Polar Front. Alternatively, a systematic warm bias of the linear calibration in the high latitude southern ocean could explain the discrepancy between TEX_{86}^L reconstructed and observed temperatures. The discrepancies can be reduced by using a non-linear TEX_{86}^L calibration developed for high latitude samples from the Southern Hemisphere.

Our findings offer insights into the potential factors governing TEX_{86}^L thermometry such as nutrient availability or archaeal community composition in high latitude regions. In the high latitude North Atlantic, regional TEX_{86}^L calibrations can be an additional option next to the global calibration, while in the high latitude Southern Ocean, the benefit of a polynomial TEX_{86}^L calibration needs to be further tested. Our studies suggest that OH-GDGTs based calibrations are also worth to be further investigated in the polar oceans. Accordingly, our study highlights that multiple approaches of global versus regional calibrations, polynomial relationships, or OH-GDGT based calibrations are beneficial to overcome the limitations of a single global TEX_{86}^L calibration in high latitude ocean regions.

Data availability

The data presented here are available on the PANGAEA database (https://doi.pangaea.de/10.1594/PANGAEA.897268).

Author contributions

EP and GM designed the study. EP measured the samples with a help of JH, analyzed the data, prepared figures and tables, and wrote the manuscript. All the authors provided feedback on the manuscript and GM reviewed the manuscript.

Competing interests

The authors declare that they have no conflict of interest.

Acknowledgments

We acknowledge the captain, crew and scientists who participated in the expeditions for collecting sediment trap samples used in this study. This project is funded through the DFG-Research Center/Cluster of Excellence "The Ocean in the Earth System" at the MARUM and supported by GLOMAR−Bremen International Graduate School for Marine Sciences, University of Bremen. The trap samples were supplied by the MARUM Centre of Marine Environmental Research at the University of Bremen (PF3) and Alfred-Wegener Institute, Helmholtz Center for Polar and Marine Sciences (FEVI16). MHI received funding for the Helmholtz Young Investigator Group SeaPump "Seasonal and regional food web interactions with the biological pump" (VH-NG-1000), the Alfred Wegener Institute for Polar and Marine Research.

References

Abbott, M. R., Richman, J. G., Nahorniak, J. S. and Barksdale, B. S.: Meanders in the Antarctic Polar Frontal Zone and their impact on phytoplankton, Deep. Res. Part II Top. Stud. Oceanogr., 48, 3891–3912, doi:10.1016/S0967-0645(01)00073-X, 2001.

Alonso-Sáez, L., Andersson, A., Heinrich, F. and Bertilsson, S.: High archaeal diversity in Antarctic circumpolar deep waters, Environ. Microbiol. Rep., 3, 689–697, doi:10.1111/j.1758-2229.2011.00282.x, 2011.

Bauerfeind, E., Nöthig, E. M., Beszczynska, A., Fahl, K., Kaleschke, L., Kreker, K., Klages, M., Soltwedel, T., Lorenzen, C. and Wegner, J.: Particle sedimentation patterns in the eastern Fram Strait during 2000-2005: Results from the Arctic long-term observatory HAUSGARTEN, Deep. Res. Part I Oceanogr. Res. Pap., 56(9), 1471–1487, doi:10.1016/j.dsr.2009.04.011, 2009.

Bauerfeind, E., Kattner, G., Ludwichowski, K.-U., Nöthig, E.-M. and Sandhop, N.: Inorganic nutrients measured on water bottle samples at AWI HAUSGARTEN during POLARSTERN cruise MSM29, , doi:10.1594/PANGAEA.834685, 2014.

Beman, J. M., Popp, B. N. and Francis, C. A.: Molecular and biogeochemical evidence for ammonia oxidation by marine Crenarchaeota in the Gulf of California, ISME J., 2, 429–441, doi:10.1038/ismej.2008.33, 2008.

5   Bendle, J. and Rosell-Melé, A.: Distributions of U^k_{37} and $U^{k\prime}_{37}$ in the surface waters and sediments of the Nordic Seas: Implications for paleoceanography, Geochemistry, Geophys. Geosystems, 5(11), 1–19, doi:10.1029/2004GC000741, 2004.

Beszczynska-Möller, A., Fahrbach, E., Rohardt, G. and Schauer, U.: Physical oceanography and current meter data from mooring F7-8, , doi:10.1594/PANGAEA.800396, 2012a.

Beszczynska-Möller, A., Fahrbach, E., Schauer, U. and Hansen, E.: Variability in Atlantic water temperature and transport at

10 the entrance to the Arctic Ocean, 1997-2010, ICES J. Mar. Sci., 69, 852–863, doi:10.1093/icejms/fss056, 2012b.

Blaga, C. I., Reichart, G. J., Heiri, O. and Sinninghe Damsté, J. S.: Tetraether membrane lipid distributions in water-column particulate matter and sediments: A study of 47 European lakes along a north-south transect, J. Paleolimnol., 41, 523–540, doi:10.1007/s10933-008-9242-2, 2009.

Chen, W., Mohtadi, M., Schefuß, E. and Mollenhauer, G.: Organic-geochemical proxies of sea surface temperature in

15 surface sediments of the tropical eastern Indian Ocean, Deep. Res. Part I Oceanogr. Res. Pap., 88, 17–29, doi:10.1016/j.dsr.2014.03.005, 2014.

Chen, W., Mohtadi, M., Schefuß, E. and Mollenhauer, G.: Concentrations and abundance ratios of long-chain alkenones and glycerol dialkyl glycerol tetraethers in sinking particles south of Java, Deep. Res. Part I Oceanogr. Res. Pap., 112, 14–24, doi:10.1016/j.dsr.2016.02.010, 2016.

20 Church, M. J., DeLong, E. F., Ducklow, H. W., Karner, M. B., Preston, C. M. and Karl, D. M.: Abundance and distribution of planktonic Archaea and Bacteria in the waters west of the Antarctic Peninsula, Limnol. Oceanogr., 48, 1893–1902, doi:10.4319/lo.2003.48.5.1893, 2003.

Conley, K. R. and Sutherland, K. R.: Particle shape impacts export and fate in the ocean through interactions with the globally abundant appendicularian Oikopleura dioica, PLoS One, 12, 1–17, doi:10.1371/journal.pone.0183105, 2017.

25 Fahrbach, E. and Cruise Participants: Report and preliminary results of the Expeditions ANTARKTIS IX/2 of the Research Vessel Polarstern in 1990/91, Punta Arenas-Cape Town, 16.11.1990-30.12-1990., 1992.

Fietz, S., Huguet, C., Rueda, G., Hambach, B. and Rosell-Melé, A.: Hydroxylated isoprenoidal GDGTs in the Nordic Seas, Mar. Chem., 152, 1–10, doi:10.1016/j.marchem.2013.02.007, 2013.

Fischer, G. and Karakaş, G.: Sinking rates and ballast composition of particles in the Atlantic Ocean: implications for the

30 organic carbon fluxes to the deep ocean, Biogeosciences, 6, 85–102, doi:10.5194/bg-6-85-2009, 2009.

Fischer, G., Gersonde, R. and Wefer, G.: Organic carbon, biogenic silica and diatom fluxes in the marginal winter sea-ice zone and in the Polar Front Region: Interannual variations and differences in composition, Deep. Res. Part II Top. Stud. Oceanogr., 49, 1721–1745, doi:10.1016/S0967-0645(02)00009-7, 2002.

Freeman, N. M. and Lovenduski, N. S.: Mapping the Antarctic Polar Front: Weekly realizations from 2002 to 2014, Earth Syst. Sci. Data, 8, 191–198, doi:10.5194/essd-8-191-2016, 2016.

Garcia, H. E., Locarnini, R. A., Boyer, T. P., Antonov, J. I., Baranova, O. K., Zweng, M. M., Reagan, J. R. and Johnson, D. R.: World Ocean Atlas 2013, Volume 4 : Dissolved Inorganic Nutrients (phosphate, nitrate, silicate), NOAA Atlas NESDIS 76, 4, 25, doi:10.1182/blood-2011-06-357442, 2013.

Gersonde, R. and Participants, C.: Report and preliminary results of the Expeditions ANTARKTIS VIII/3 of the Research Vessel Polarstern in 1989/90, Cape Town-Punta Arenas, 01.11.1989-01.12-1989. [online] Available from: http://epic.awi.de/29793/1/PE_17.pdf, 1990.

Hebbeln, D.: Flux of ice-rafted detritus from sea ice in the Fram Strait, Deep. Res. Part II Top. Stud. Oceanogr., 47, 1773–1790, doi:10.1016/S0967-0645(00)00006-0, 2000.

Hebbeln, D. and Wefer, G.: Effects of ice coverage and ice-rafted material on sedimentation in the Fram Strait, Nature, 350, 409–411, doi:10.1038/350409a0, 1991.

Herfort, L., Schouten, S., Abbas, B., Veldhuis, M. J. W., Coolen, M. J. L., Wuchter, C., Boon, J. P., Herndl, G. J. and Sinninghe Damsté, J. S.: Variations in spatial and temporal distribution of Archaea in the North Sea in relation to environmental variables, FEMS Microbiol. Ecol., 62(3), 242–257, doi:10.1111/j.1574-6941.2007.00397.x, 2007.

Ho, S. L., Mollenhauer, G., Fietz, S., Martínez-Garcia, A., Lamy, F., Rueda, G., Schipper, K., Méheust, M., Rosell-Melé, A., Stein, R. and Tiedemann, R.: Appraisal of TEX_{86} and TEX_{86}^{L} thermometries in subpolar and polar regions, Geochim. Cosmochim. Acta, 131, 213–226, doi:10.1016/j.gca.2014.01.001, 2014.

Hopmans, E. C., Schouten, S., Pancost, R. D., Van Der Meer, M. T. J. and Sinninghe Damsté, J. S.: Analysis of intact tetraether lipids in archaeal cell material and sediments by high performance liquid chromatography/atmospheric pressure chemical ionization mass spectrometry, Rapid Commun. Mass Spectrom., 14, 585–589, doi:10.1002/(SICI)1097-0231(20000415)14:7<585::AID-RCM913>3.0.CO;2-N, 2000.

Hopmans, E. C., Weijers, J. W. H., Schefuß, E., Herfort, L., Sinninghe Damsté, J. S. and Schouten, S.: A novel proxy for terrestrial organic matter in sediments based on branched and isoprenoid tetraether lipids, Earth Planet. Sci. Lett., 224, 107–116, doi:10.1016/j.epsl.2004.05.012, 2004.

Horak, R. E. A., Qin, W., Bertagnolli, A. D., Nelson, A., Heal, K. R., Han, H., Heller, M., Schauer, A. J., Jeffrey, W. H., Armbrust, E. V., Moffett, J. W., Ingalls, A. E., Stahl, D. A. and Devol, A. H.: Relative impacts of light, temperature, and reactive oxygen on thaumarchaeal ammonia oxidation in the North Pacific Ocean, Limnol. Oceanogr., 63(2), 1–16, doi:10.1002/lno.10665, 2017.

Huguet, C., Cartes, J. E., Sinninghe Damsté, J. S. and Schouten, S.: Marine crenarchaeotal membrane lipids in decapods: Implications for the TEX_{86} paleothermometer, Geochemistry, Geophys. Geosystems, 7, Q11010, doi:10.1029/2006GC001305, 2006.

Huguet, C., Schimmelmann, A., Thunell, R., Lourens, L. J., Sinninghe Damsté, J. S. and Schouten, S.: A study of the TEX$_{86}$ paleothermometer in the water column and sediments of the Santa Barbara Basin, California, Paleoceanography, 22, PA3203, doi:10.1029/2006PA001310, 2007.

Huguet, C., Fietz, S. and Rosell-Melé, A.: Global distribution patterns of hydroxy glycerol dialkyl glycerol tetraethers, Org.
5 Geochem., 57, 107–118, doi:10.1016/j.orggeochem.2013.01.010, 2013.

Hurley, S. J., Elling, F. J., Könneke, M., Buchwald, C., Wankel, S. D., Santoro, A. E., Lipp, J. S., Hinrichs, K.-U. and Pearson, A.: Influence of ammonia oxidation rate on thaumarchaeal lipid composition and the TEX$_{86}$ temperature proxy, Proc. Natl. Acad. Sci. USA, 113(28), 7762–7767, doi:10.1073/pnas.1518534113, 2016.

Inglis, G. N., Farnsworth, A., Lunt, D., Foster, G. L., Hollis, C. J., Pagani, M., Jardine, P. E., Pearson, P. N., Markwick, P.
10 and Galsworthy, A. M. J.: Descent toward the Icehouse: Eocene sea surface cooling inferred from GDGT distributions, Paleoceanography, 30, 1000–1020, doi:10.1002/2014PA002723.Received, 2015.

Iversen, M. H. and Ploug, H.: Ballast minerals and the sinking carbon flux in the ocean: carbon-specific respiration rates and sinking velocity of marine snow aggregates, Biogeosciences, 7, 2613–2624, doi:10.5194/bg-7-2613-2010, 2010.

Iversen, M. H., Nowald, N., Ploug, H., Jackson, G. a. and Fischer, G.: High resolution profiles of vertical particulate organic
15 matter export off Cape Blanc, Mauritania: Degradation processes and ballasting effects, Deep. Res. Part I Oceanogr. Res. Pap., 57(6), 771–784, doi:10.1016/j.dsr.2010.03.007, 2010.

Iversen, M. H., Pakhomov, E. A., Hunt, B. P. V., van der Jagt, H., Wolf-Gladrow, D. and Klaas, C.: Sinkers or floaters? Contribution from salp pellets to the export flux during a large bloom event in the Southern Ocean, Deep. Res. Part II Top. Stud. Oceanogr., 138(December 2016), 116–125, doi:10.1016/j.dsr2.2016.12.004, 2017.

20 Jackson, G. A. and Checkley Jr, D. M.: Particle size distribution in the upper 100 m water column and their implications for animal feeding in the plankton, Deep Sea Res. Part I Oceanogr. Res. Pap., 58, 283–297, doi:10.1016/j.dsr.2010.12.008, 2011.

Kattner, G. and Participants, C.: Reports on Polar and Marine Research. The Expedition of the Research Vessel Polarstern to the Arctic in 2008 (ARK-XXIII/2), Longyearbyen-Reykjavik, 06.07-10.08.2008. [online] Available from: http://epic.awi.de/28933/1/Kat2009b.pdf, 2009.

25 Kim, J.-H., van der Meer, J., Schouten, S., Helmke, P., Willmott, V., Sangiorgi, F., Koç, N., Hopmans, E. C. and Sinninghe Damsté, J. S.: New indices and calibrations derived from the distribution of crenarchaeal isoprenoid tetraether lipids: Implications for past sea surface temperature reconstructions, Geochim. Cosmochim. Acta, 74, 4639–4654, doi:10.1016/j.gca.2010.05.027, 2010.

Kim, J.-H., Schouten, S., Rodrigo-Gámiz, M., Rampen, S., Marino, G., Huguet, C., Helmke, P., Buscail, R., Hopmans, E. C.,
30 Pross, J., Sangiorgi, F., Middelburg, J. B. M. and Sinninghe Damsté, J. S.: Influence of deep-water derived isoprenoid tetraether lipids on the TEX$_{86}^{H}$ paleothermometer in the Mediterranean Sea, Geochim. Cosmochim. Acta, 150, 125–141, doi:10.1016/j.gca.2014.11.017, 2015.

Kim, J. H., Crosta, X., Michel, E., Schouten, S., Duprat, J. and Sinninghe Damsté, J. S.: Impact of lateral transport on organic proxies in the Southern Ocean, Quat. Res., 71(2), 246–250, doi:10.1016/j.yqres.2008.10.005, 2009.

Klages, M. and Participants, C.: Reports on Polar and Marine Research, The Expedition of the Research Vessel Polarstern to the Arctic in 2007 (ARK-XXII/1a-c, Bremerhaven-Tromso-Longyarbyen-Tromso, 29.05-25.07.2007, Alfred-Wegener Institute. [online] Available from: http://epic.awi.de/29744/1/Kla2011a.pdf, 2007.

Könneke, M., Bernhard, A. E., de la Torre, J. R., Walker, C. B., Waterbury, J. B. and Stahl, D. A.: Isolation of an autotrophic ammonia-oxidizing marine archaeon, Nature, 437, 543–546, doi:10.1038/nature03911, 2005.

Lalande, C., Bauerfeind, E., Nöthig, E. M. and Beszczynska-Möller, A.: Impact of a warm anomaly on export fluxes of biogenic matter in the eastern Fram Strait, Prog. Oceanogr., 109, 70–77, doi:10.1016/j.pocean.2012.09.006, 2013.

Lalande, C., Nöthig, E. M., Bauerfeind, E., Hardge, K., Beszczynska-Möller, A. and Fahl, K.: Lateral supply and downward export of particulate matter from upper waters to the seafloor in the deep eastern Fram Strait, Deep. Res. Part I Oceanogr. Res. Pap., 114, 78–89, doi:10.1016/j.dsr.2016.04.014, 2016.

Laubscher, R. K., Prissinotto, R. and McQuaid, C. D.: Phytoplankton production and biomass at frontal zones in the Atlantic sector of the Southern Ocean, Polar Biol., 13, 471–481, 1993.

Lee, K. E., Kim, J.-H., Wilke, I., Helmke, P. and Schouten, S.: A study of the alkenone, TEX_{86}, and planktonic foraminifera in the Benguela Upwelling System: Implications for past sea surface temperature estimates, Geochemistry, Geophys. Geosystems, 9(10), 1–19, doi:10.1029/2008GC002056, 2008.

Lincoln, S. A., Wai, B., Eppley, J. M., Church, M. J., Summons, R. E. and DeLong, E. F.: Planktonic Euryarchaeota are a significant source of archaeal tetraether lipids in the ocean, Proc. Natl. Acad. Sci. USA, 111(27), 9858–9863, doi:10.1073/pnas.1409439111, 2014.

Liu, X. L., Lipp, J. S., Simpson, J. H., Lin, Y. S., Summons, R. E. and Hinrichs, K. U.: Mono- and dihydroxyl glycerol dibiphytanyl glycerol tetraethers in marine sediments: Identification of both core and intact polar lipid forms, Geochim. Cosmochim. Acta, 89, 102–115, doi:10.1016/j.gca.2012.04.053, 2012.

Locarnini, R. A., Mishonov, A. V., Antonov, J. I., Boyer, T. P., Garcia, H. E., Baranova, O. K., Zweng, M. M., Paver, C. R., Reagan, J. R., Johnson, D. R., Hamilton, M. and Seidov, D.: World Ocean Atlas 2013, Volume 1: Temperature, S. Levitus, Ed.; A. Mishonov, Tech. Ed.; NOAA Atlas NESDIS, 73, 40, doi:10.1182/blood-2011-06-357442, 2013.

López-García, P., Rodriguez-Valera, F., Pedrós-Alió, C. and Moreira, D.: Unexpected diversity of small eukaryotes in deep-sea Antarctic plankton, Nature, 409(6820), 603–607, doi:10.1038/35054537, 2001.

Lü, X., Liu, X. L., Elling, F. J., Yang, H., Xie, S., Song, J., Li, X., Yuan, H., Li, N. and Hinrichs, K. U.: Hydroxylated isoprenoid GDGTs in Chinese coastal seas and their potential as a paleotemperature proxy for mid-to-low latitude marginal seas, Org. Geochem., 89–90, 31–43, doi:10.1016/j.orggeochem.2015.10.004, 2015.

Manley, T. O.: Branching of Atlantic Water within the Greenland-Spitsbergen Passage: An estimate of recirculation, J. Geophys. Res., 100, 20627–20634, doi:10.1029/95JC01251, 1995.

Martin-Cuadrado, A.-B., Rodriguez-Valera, F., Moreira, D., Alba, J. C., Ivars-Martínez, E., Henn, M. R., Talla, E. and López-García, P.: Hindsight in the relative abundance, metabolic potential and genome dynamics of uncultivated marine

archaea from comparative metagenomic analyses of bathypelagic plankton of different oceanic regions, ISME J., 2, 865–886, doi:10.1038/ismej.2008.40, 2008.

Meyer, V. D., Max, L., Hefter, J., Tiedemann, R. and Mollenhauer, G.: Glacial-to-Holocene evolution of sea surface temperature and surface circulation in the subarctic northwest Pacific and the Western Bering Sea, Paleoceanography, 31, 916–927, doi:10.1002/2015PA002877, 2016.

Mollenhauer, G., Eglinton, T. I., Hopmans, E. C. and Sinninghe Damsté, J. S.: A radiocarbon-based assessment of the preservation characteristics of crenarchaeol and alkenones from continental margin sediments, Org. Geochem., 39, 1039–1045, doi:10.1016/j.orggeochem.2008.02.006, 2008.

Mollenhauer, G., Basse, A., Kim, J.-H., Sinninghe Damsté, J. S. and Fischer, G.: A four-year record of $U^{k'}_{37}$- and TEX_{86}-derived sea surface temperature estimates from sinking particles in the filamentous upwelling region off Cape Blanc, Mauritania, Deep. Res. Part I Oceanogr. Res. Pap., 97, 67–79, doi:10.1016/j.dsr.2014.11.015, 2015.

Moore, J. K. and Abbott, M. R.: Phytoplankton chlorophyll distributions and primary production in the Southern Ocean, J. Geophys. Res. Ocean., 105, 28,709-28,722, doi:10.1029/1999JC000043, 2000.

Moore, J. K. and Abbott, M. R.: Surface chlorophyll concentrations in relation to the Antarctic Polar Front: seasonal and spatial patterns from satellite observations, J. Mar. Syst., 37, 69–86, doi:10.1016/S0924-7963(02)00196-3, 2002.

Moore, J. K., Abbott, M. R. and Richman, J. G.: Location and dynamics of the Antarctic Polar Front from satellite sea surface temperature data, J. Geophys. Res., 102, 3059–3074, doi:10.1029/97JC01705, 1999.

Moreau, R. A., Whitaker, B. D. and Hicks, K. B.: Phytosterols, phytostanols, and their conjugates in foods: structural diversity, quantitative analysis, and health-promoting uses, Prog. Lipid Res., 41, 457–500, doi:10.1016/S0163-7827(02)00006-1, 2002.

Moreira, D., Rodríguez-Valera, F. and López-García, P.: Analysis of a genome fragment of a deep-sea uncultivated Group II euryarchaeote containing 16S rDNA, a spectinomycin-like operon and several energy metabolism genes, Environ. Microbiol., 6(9), 959–969, doi:10.1111/j.1462-2920.2004.00644.x, 2004.

Müller, P. J. and Fischer, G.: C37-Alkenones as Paleotemperature Tool: Fundamentals Based on Sediment Traps and Surface Sediments from the South Atlantic Ocean, in The South Atlantic in the Late Quaternary, edited by G. Wefer, S. Mulitza, and V. Ratmeyer, pp. 167–193, Springer, Berlin, Heidelberg., 2003.

Murray, A. E., Wul, K. Y., Moyer, C. L., Karl, D. M. and Delong, E. F.: Evidence for Circumpolar Distribution of Planktonic Archaea in the Southern Ocean, Aquat. Microb. Ecol., 18, 263–273, 1999.

Nöthig, E.-M., Bracher, A., Engel, A., Metfies, K., Niehoff, B., Peeken, I., Bauerfeind, E., Cherkasheva, A., Gäbler-Schwarz, S., Hardge, K., Kilias, E., Kraft, A., Kidane, Y. M., Lalande, C., Piontek, J., Thomisch, K. and Wurst, M.: Summertime plankton ecology in Fram Strait-a compilation of long-and short-term observations, Polar Res., 34, 1–18, doi:10.3402/polar.v34.23349, 2015.

Orsi, A. H., Whitworth III, T. and Nowlin Jr, W. D.: On the meridional extent and fronts of the Antarctic Circumpolar Current, Deep. Res. Part I Oceanogr. Res. Pap., 42, 641–673, doi:10.1016/0967-0637(95)00021-W, 1995.

Park, E., Hefter, J., Fischer, G. and Mollenhauer, G.: TEX_{86} in sinking particles in three eastern Atlantic upwelling regimes, Org. Geochem., 124, 151–163, doi:10.1016/j.orggeochem.2018.07.015, 2018.

Pitcher, A., Wuchter, C., Siedenberg, K., Schouten, S. and Sinninghe Damsté, J. S.: Crenarchaeol tracks winter blooms of ammonia-oxidizing Thaumarchaeota in the coastal North Sea, Limnol. Oceanogr., 56, 2308–2318, doi:10.4319/lo.2011.56.6.2308, 2011.

Ploug, H., Iversen, M. H. and Fischer, G.: Ballast, sinking velocity, and apparent diffusivity within marine snow and zooplankton fecal pellets: Implications for substrate turnover by attached bacteria, Limnol. Oceanogr., 53(5), 1878–1886, doi:10.4319/lo.2008.53.5.1878, 2008a.

Ploug, H., Iversen, M. H., Koski, M. and Buitenhuis, E. T.: Production, oxygen respiration rates, and sinking velocity of copepod fecal pellets: Direct measurements of ballasting by opal and calcite, Limnol. Oceanogr., 53(2), 469–476, doi:10.4319/lo.2008.53.2.0469, 2008b.

Read, J. F., Pollard, R. T. and Bathmann, U.: Physical and biological patchiness of an upper ocean transect from South Africa to the ice edge near the Greenwich Meridian, Deep. Res. Part II Top. Stud. Oceanogr., 49, 3713–3733, doi:10.1016/S0967-0645(02)00108-X, 2002.

Reynolds, R. W., Smith, T. M., Liu, C., Chelton, D. B., Casey, K. S. and Schlax, M. G.: Daily high-resolution-blended analyses for sea surface temperature, J. Clim., 20(22), 5473–5496, doi:10.1175/2007JCLI1824.1, 2007.

Richey, J. N. and Tierney, J. E.: GDGT and alkenone flux in the northern Gulf of Mexico: Implications for the TEX_{86} and $U^{k'}_{37}$ paleothermometers, Paleoceanography, 31, 1547–1561, doi:10.1002/2016PA003032, 2016.

Rodrigo-Gámiz, M., Rampen, S. W., de Haas, H., Baas, M., Schouten, S. and Sinninghe Damsté, J. S.: Constraints on the applicability of the organic temperature proxies $U^{k'}_{37}$, TEX_{86} and LDI in the subpolar region around Iceland, Biogeosciences, 12, 6573–6590, doi:10.5194/bgd-12-6573-2015, 2015.

Schlitzer, R.: Ocean Data View, odv.awi.de [online] Available from: odv.awi.de, 2017.

Schouten, S., Hopmans, E. C., Schefuß, E. and Damsté, J. S. S.: Distributional variations in marine crenarchaeotal membrane lipids: a new tool for reconstructing ancient sea water temperatures?, Earth Planet. Sci. Lett., 204, 265–274, doi:doi.org/10.1016/S0012-821X(02)00979-2, 2002.

Schouten, S., van der Meer, M. T. J., Hopmans, E. C. and Sinninghe Damsté, J. S.: Comment on "Lipids of marine Archaea: Patterns and provenance in the water column and sediments" by Turich et al. (2007), Geochim. Cosmochim. Acta, 72, 5342–5346, doi:10.1016/j.gca.2008.03.028, 2008.

Schouten, S., Villanueva, L., Hopmans, E. C., van der Meer, M. T. J. and Sinninghe Damsté, J. S.: Are Marine Group II Euryarchaeota significant contributors to tetraether lipids in the ocean?, Proc. Natl. Acad. Sci. U. S. A., 111(41), E4285, doi:10.1073/pnas.1416176111, 2014.

Seki, O., Bendle, J. A., Harada, N., Kobayashi, M., Sawada, K., Moossen, H., Inglis, G. N., Nagao, S. and Sakamoto, T.: Assessment and calibration of TEX_{86} paleothermometry in the Sea of Okhotsk and sub-polar North Pacific region: Implications for paleoceanography, Prog. Oceanogr., 126, 254–266, doi:10.1016/j.pocean.2014.04.013, 2014.

Shevenell, A. E., Ingalls, A. E., Domack, E. W. and Kelly, C.: Holocene Southern Ocean surface temperature variability west of the Antarctic Peninsula, Nature, 470, 250–254, doi:10.1038/nature09751, 2011.

Sluijs, A., Schouten, S., Pagani, M., Woltering, M., Brinkhuis, H., Damsté, J. S. S., Dickens, G. R., Huber, M., Reichart, G.-J., Stein, R., Matthiessen, J., Lourens, L. J., Pedentchouk, N., Backman, J., Moran, K. and the Expedition 302 Scientists:

5   Subtropical Arctic Ocean temperatures during the Palaeocene/Eocene thermal maximum, Nature, 441, 610–613, doi:10.1038/nature04668, 2006.

Soltwedel, T., Bauerfeind, E., Bergmann, M., Bracher, A., Budaeva, N., Busch, K., Cherkasheva, A., Fahl, K., Grzelak, K., Hasemann, C., Jacob, M., Kraft, A., Lalande, C., Metfies, K., Nöthig, E. M., Meyer, K., Quéric, N. V., Schewe, I., Włodarska-Kowalczuk, M. and Klages, M.: Natural variability or anthropogenically-induced variation? Insights from 15

10   years of multidisciplinary observations at the arctic marine LTER site HAUSGARTEN, Ecol. Indic., 65, 89–102, doi:10.1016/j.ecolind.2015.10.001, 2016.

Taylor, K. W. R., Huber, M., Hollis, C. J., Hernandez-Sanchez, M. T. and Pancost, R. D.: Re-evaluating modern and Palaeogene GDGT distributions: Implications for SST reconstructions, Glob. Planet. Change, 108, 158–174, doi:10.1016/j.gloplacha.2013.06.011, 2013.

15   Tierney, J. E. and Tingley, M. P.: A TEX_{86} surface sediment database and extended Bayesian calibration, Sci. data, 2, 150029, doi:10.1038/sdata.2015.29, 2015.

Tolar, B. B., Ross, M. J., Wallsgrove, N. J., Liu, Q., Aluwihare, L. I., Popp, B. N. and Hollibaugh, J. T.: Contribution of ammonia oxidation to chemoautotrophy in Antarctic coastal waters, ISME J., 10, 2605–2619, doi:10.1038/ismej.2016.61, 2016.

20   Turich, C., Freeman, K. H., Bruns, M. A., Conte, M., Jones, A. D. and Wakeham, S. G.: Lipids of marine Archaea: Patterns and provenance in the water-column and sediments, Geochim. Cosmochim. Acta, 71, 3272–3291, doi:10.1016/j.gca.2007.04.013, 2007.

Walczowski, W.: Frontal structures in the West Spitsbergen current margins, Ocean Sci., 9, 957–975, doi:10.5194/os-9-957-2013, 2013.

25   Walter, H. J., Geibert, W., Rutgers Van Der Loeff, M. M., Fischer, G. and Bathmann, U.: Shallow vs. deep-water scavenging of [231]Pa and [230]Th in radionuclide enriched waters of the Atlantic sector of the Southern Ocean, Deep. Res. Part I Oceanogr. Res. Pap., 48, 471–493, doi:10.1016/S0967-0637(00)00046-7, 2001.

Wassmann, P., Reigstad, M., Haug, T., Rudels, B., Carroll, M. L., Hop, H., Gabrielsen, G. W., Falk-Petersen, S., Denisenko, S. G., Arashkevich, E., Slagstad, D. and Pavlova, O.: Food webs and carbon flux in the Barents Sea, Prog. Oceanogr., 71(2–

30   4), 232–287, doi:10.1016/j.pocean.2006.10.003, 2006.

Weijers, J. W. H., Schouten, S., Spaargaren, O. C. and Sinninghe Damsté, J. S.: Occurrence and distribution of tetraether membrane lipids in soils: Implications for the use of the TEX_{86} proxy and the BIT index, Org. Geochem., 37, 1680–1693, doi:10.1016/j.orggeochem.2006.07.018, 2006.

Weijers, J. W. H., Lim, K. L. H., Aquilina, A., Damsté, J. S. S. and Pancost, R. D.: Biogeochemical controls on glycerol dialkyl glycerol tetraether lipid distributions in sediments characterized by diffusive methane flux, Geochemistry, Geophys. Geosystems, 12(10), 1–15, doi:10.1029/2011GC003724, 2011.

Wekerle, C., Krumpen, T., Dinter, T., von Appen, W.-J., Iversen, M. H. and Salter, I.: Properties of Sediment Trap Catchment Areas in Fram Strait: Results From Lagrangian Modeling and Remote Sensing, Front. Mar. Sci., 5(November), doi:10.3389/fmars.2018.00407, 2018.

Wuchter, C., Abbas, B., Coolen, M. J. L., Herfort, L., van Bleijswijk, J., Timmers, P., Strous, M., Teira, E., Herndl, G. J., Middelburg, J. J., Schouten, S. and Sinninghe Damsté, J. S.: Archaeal nitrification in the ocean., Proc. Natl. Acad. Sci. USA, 103, 12317–12322, doi:10.1073/pnas.0701630104, 2006a.

Wuchter, C., Schouten, S., Wakeham, S. G. and Sinninghe Damsté, J. S.: Archaeal tetraether membrane lipid fluxes in the northeastern Pacific and the Arabian Sea: Implications for TEX_{86} paleothermometry, Paleoceanography, 21, 1–9, doi:10.1029/2006PA001279, 2006b.

Yamamoto, M., Shimamoto, A., Fukuhara, T., Tanaka, Y. and Ishizaka, J.: Glycerol dialkyl glycerol tetraethers and TEX_{86} index in sinking particles in the western North Pacific, Org. Geochem., 53, 52–62, doi:10.1016/j.orggeochem.2012.04.010, 2012.

Zhang, Y. G., Zhang, C. L., Liu, X.-L., Li, L., Hinrichs, K.-U. and Noakes, J. E.: Methane Index: A tetraether archaeal lipid biomarker indicator for detecting the instability of marine gas hydrates, Earth Planet. Sci. Lett., 307, 525–534, doi:10.1016/j.epsl.2011.05.031, 2011.

Zhang, Y. G., Pagani, M. and Wang, Z.: Ring Index: A new strategy to evaluate the integrity of TEX_{86} paleothermometry, Paleoceanography, 31(2), 220–232, doi:10.1002/2015PA002848, 2016.

Table 1. Information on FEVI16 and PF3 trap.

Trap name	FEVI16	PF3
Region	Eastern Fram Strait	Antarctic Polar Front
Location		
Latitude (° N)	79.02	-50.13
Longitude (° E)	4.35	5.83
Water depth (m)	2580	3785
Trap depth (m)	1296	614
		3196
Deployment period (dd.mm.yyyy)		
Start	23.07.2007	10.11.1989
End	30.06.2008	23.12.1990
Sampling interval (d)	10-31	21, 42*
Cruise reports	ARK-XXII/1c (Klages and Participants, 2007)	ANT-VIII/3 (Gersonde and Participants, 1990)
	ARK-XXIII/2 (Kattner and Participants, 2009)	ANT-IX/2 (Fahrbach and Cruise Participants, 1992)

*The exact sampling interval of each sample at FEVI and PF3 can be found on PANGAEA (https://doi.pangaea.de/10.1594/PANGAEA.897268).

Table 2. Summary of TEX_{86}^L thermometry in FEVI16 and PF3 site.

Trap name	FEVI16	PF3
Oceanographic setting	Seasonal ice cover	Winter ice edge
Main GDGTs producer	Thaumarchaeota	Thaumarchaeota + Euryarchaeota
Surface ocean temperature	[a]Satellite-SST: -0.1 − 3.4 °C [b]Ave. SST: 1.9 °C	[a]Satellite-SST: 1.8 − 5.2 °C [b]Ave. SST: 3.5 °C
Shallow trap	[c]TEX_{86}^L T: 2.8 °C (30 − 80 m depth signal)	[c]TEX_{86}^L T: 4.6 °C (Thaumarchaeota + Euryarchaeota)
Deep trap		[c]TEX_{86}^L T: 8.5 °C (Dominant Euryarchaeota)
Surface sediment	TEX_{86}^L T: 2.3/2.8 °C at 2400 m	TEX_{86}^L T: 9.1°C at 3800 m
Relevant processes for GDGTs	- Export of upper ocean signal by fast settling particles - Highly ballasted with opal and carbonate [d]s.v.: 15 m d^{-1}	- Contribution of Euryarchaeota in [e]CDW casing warm biases
Conclusions	- Linear calibration (TEX_{86}^L) applicable - Temporal offset due to changing ballast materials and s.v. - OH-GDGTs based calibrations applicable	- Linear calibration (TEX_{86}^L) unreliable - Nonlinear relationship between TEX_{86}^L and SST (>50° N) - OH-GDGTs based calibrations applicable

[a]Satellite-derived sea surface temperature
[b]Averaged surface temperature over the trap deployment period
[c]Flux-weighted average temperature over the trap deployment period
[d]s.v.: sinking velocity
[e]CDW: Circumpolar Deep Water
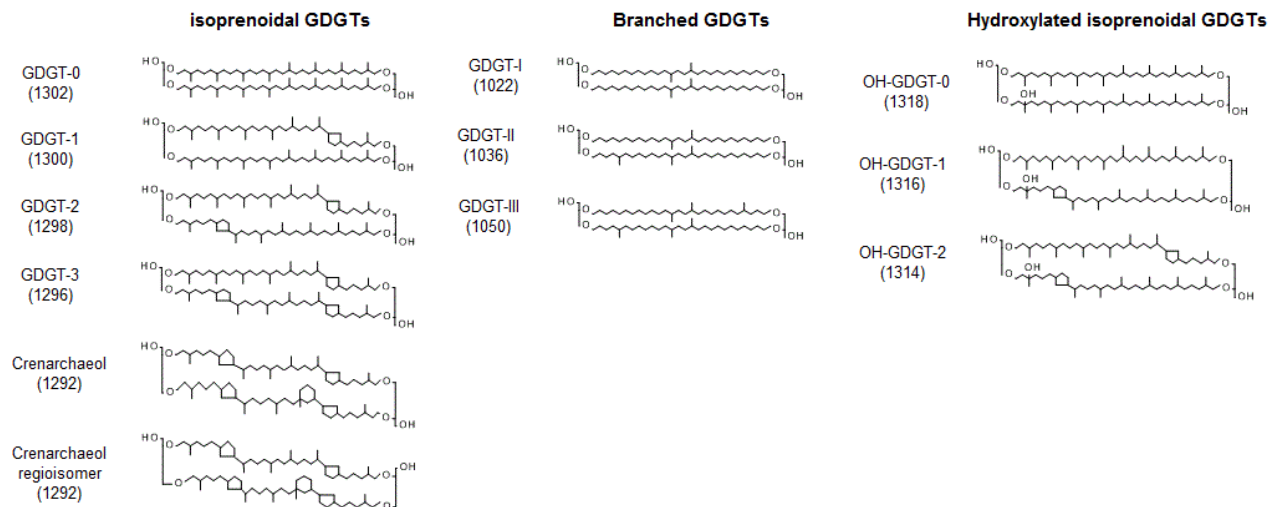
Figure 1. Chemical structures and molecular ion m/z values of the isoprenoid glycerol dialkyl glycerol tetraethers (GDGTs), branched GDGTs, and hydroxylated GDGTs.
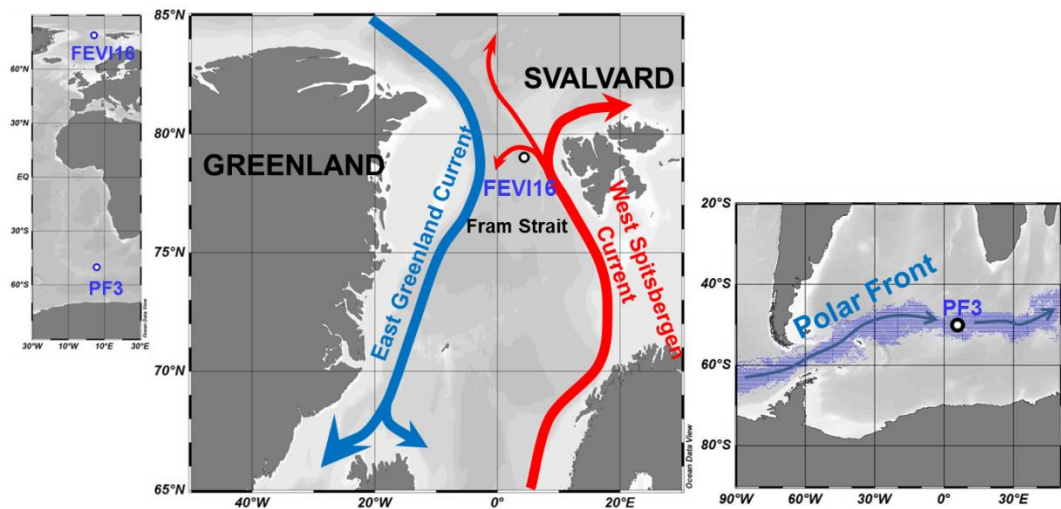
Figure 2. Map of sediment trap locations in high northern latitude (FEVI16) and in Antarctic Polar Front (PF3). In Fram Strait, the northward red arrow represents the West Spitsbergen Current bringing warm and saline Atlantic Waters to the Arctic and the southward blue arrow displays the East Greenland Current transporting cold and fresh water to the Norwegian Sea. Around the Antarctic, the digitized blue shadow exhibits the location of the Antarctic Polar Front for the year 2002-2014 at weekly resolution (Freeman and Lovenduski, 2016). The blue arrow indicates the clockwise Antarctic Circumpolar Current. Ocean Data View is used for mapping (Schlitzer, 2017; available at https://odv.awi.de).
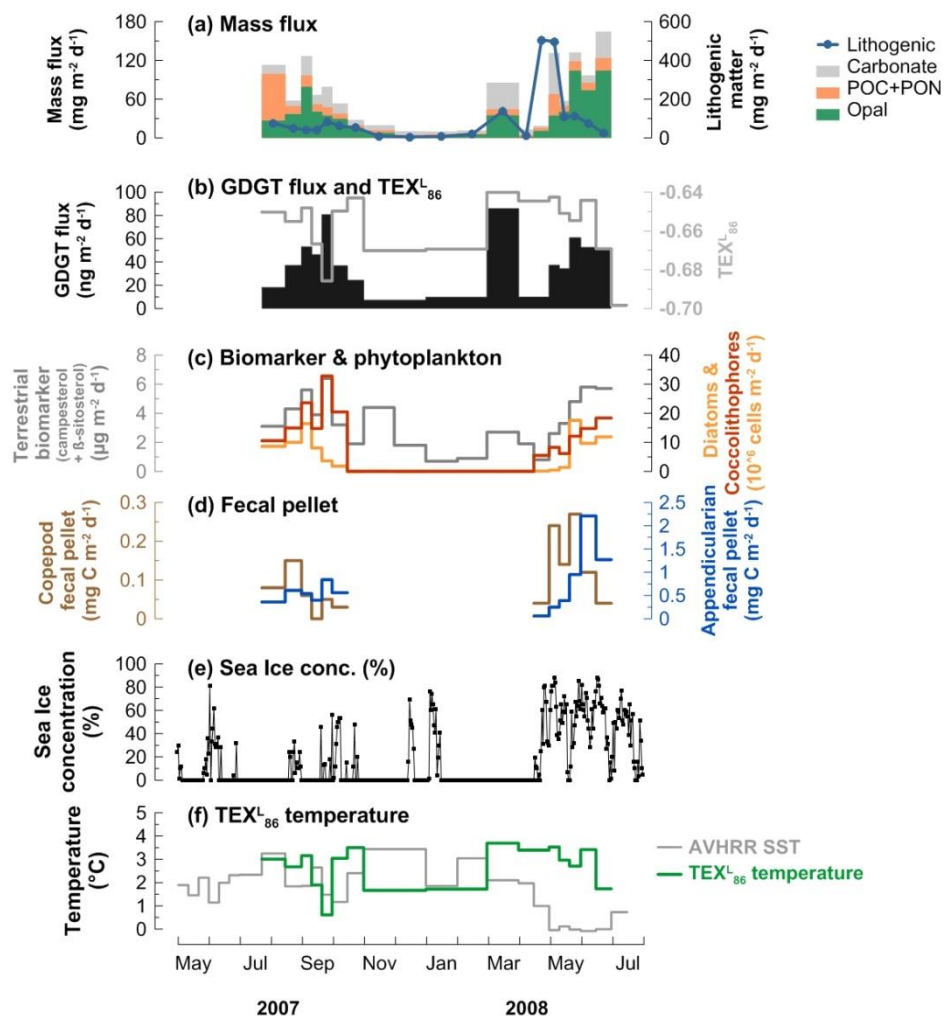
Figure 3. Changes in mass flux (a), GDGT flux (b), terrestrial biomarker flux and diatom and coccolithophore abundances (c), fecal pellet flux (d), Sea ice concentration (e), TEX$_{86}^{L}$-derived temperatures and satellite-derived SSTs obtained at 79.125° N, 4.375° E near the trap site (f) at 1296 m water depth in the eastern Fram Strait site, FEVI16 during the deployment period (July 2007−July 2008). (a), (c), (d), and (e) are previously reported by Lalande et al., (2016).
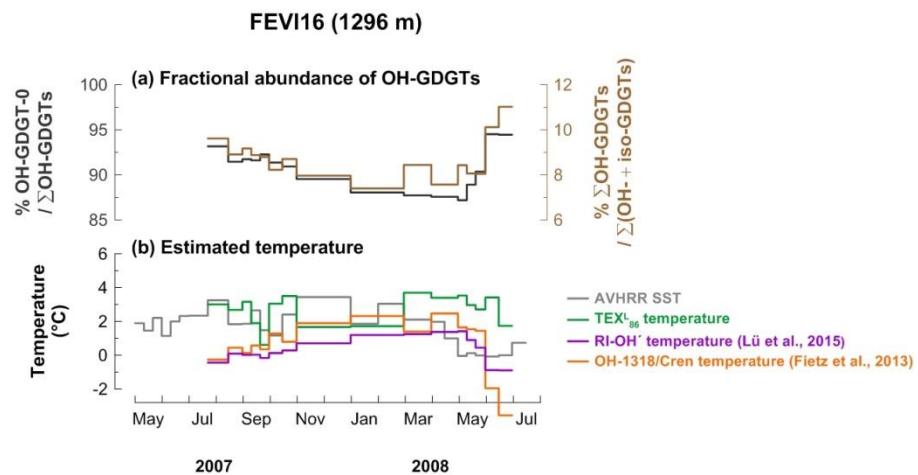
Figure 4. Changes in fractional abundance of OH-GDGTs (a) and estimated temperatures based on OH-related calibrations (b) at site FEVI16. The purple and orange lines indicate the calculated temperatures using the calibrations by Fietz et al., (2013) (Eq. 4) and Lü et al., (2015) (Eq. 6), respectively. The green line indicates the TEX_{86}^L-derived temperatures.
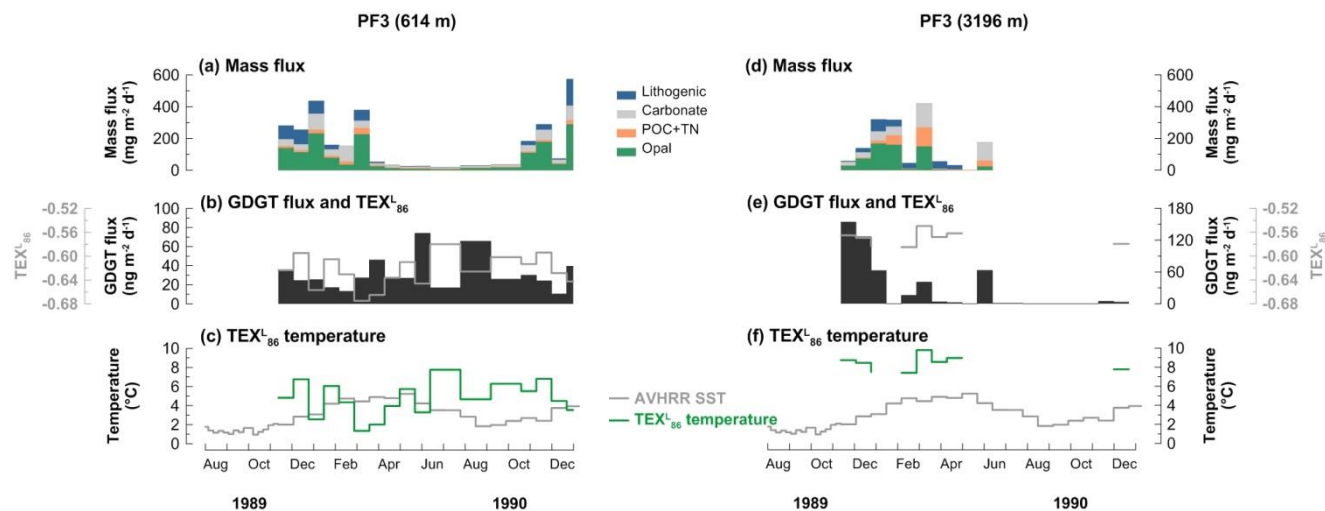
Figure 5. Changes in mass flux (a, d), GDGT flux (b, e) and TEX$^L_{86}$-derived temperatures and satellite-derived SSTs obtained at 50.125° S, 5.875° E near the trap site (c, f) at the 614 m (left panels) and 3196 m (right panels) water depth in the Antarctic Polar Front site (PF3) during the deployment period (November 1989−December 1990).
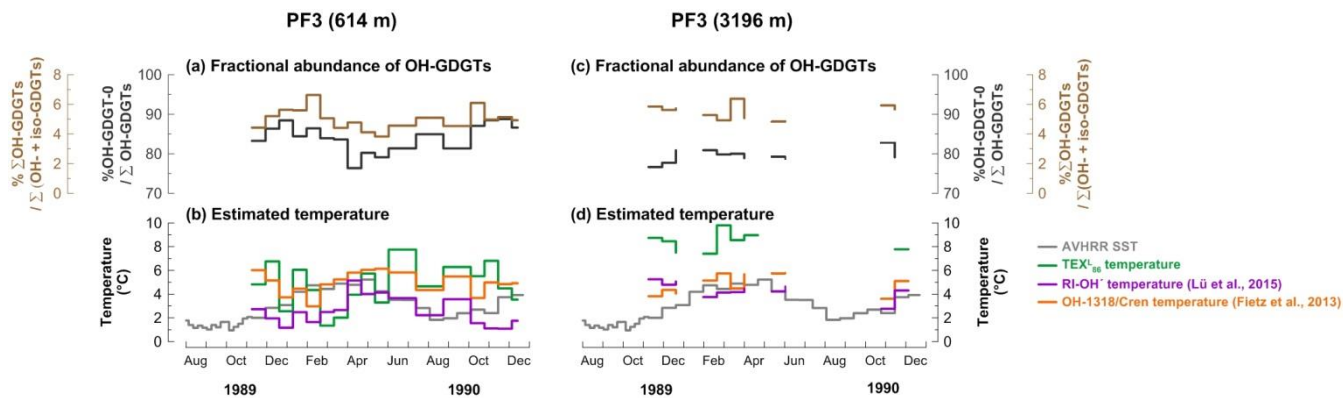
Figure 6. Changes in fractional abundance of OH-GDGTs (a, c) and estimated temperatures based on OH-related calibrations (b, d) at site PF3. The purple and orange lines indicate the calculated temperatures using the calibrations by Fietz et al., (2013) (Eq. 4) and Lü et al., (2015) (Eq. 6), respectively. The green lines indicate the TEX_{86}^L-derived temperatures.
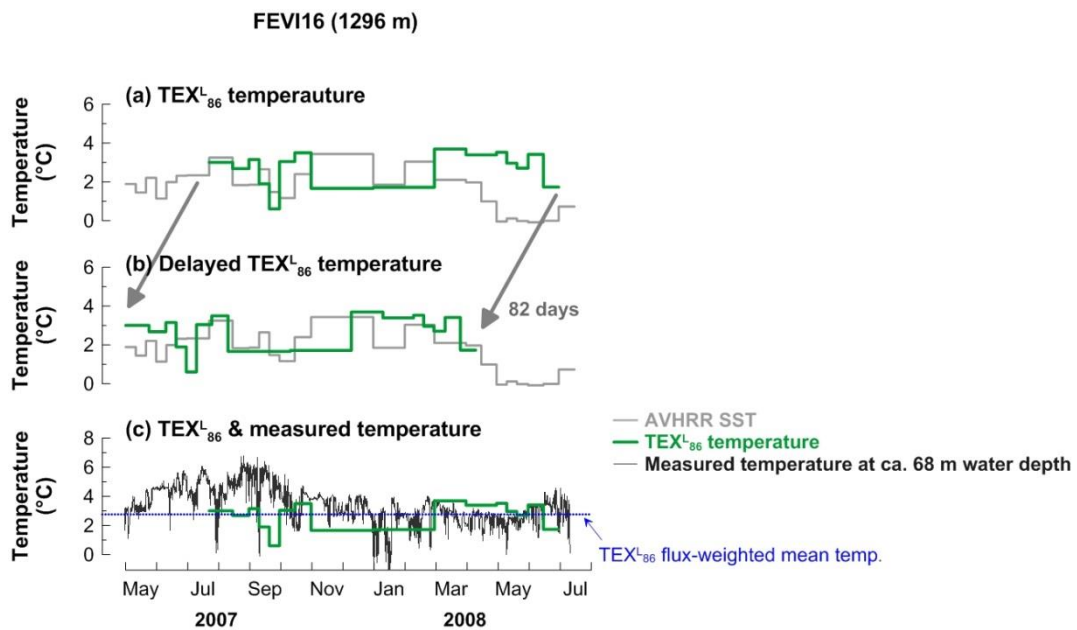
Figure 7. Changes in TEX$_{86}^{L}$-derived temperatures and satellite-derived SSTs (a), time-delayed TEX$_{86}^{L}$ temperatures (b), sensor measured temperatures at approximately 68 m water depth at site FEVI16.
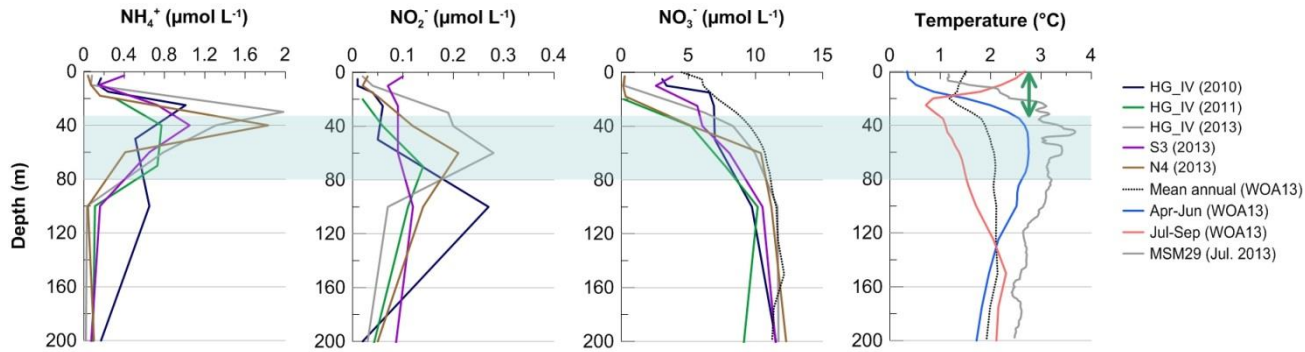
Figure 8. Depth profiles of nutrient concentration (NH$_4^+$, NO$_2^-$, NO$_3^-$), and temperature in the Fram Strait. The navy, green, and gray lines represent the central station of the Long-Term Ecological Research (LTER) observatory HAUSGARTEN (HG-IV), close to FEVI16 trap location. The purple and brown lines represent the southern and northern stations of HG-IV. Black dotted lines for NO$_3^-$ and temperature, and blue and orange lines for temperature represent the data sets extracted from WOA13. Only two seasonal profiles (April to June and July to September) from WOA13 are available at the same location (79.125° N, 4.375° E) near the site FEVI16. Measured nutrient concentrations are reported on PANGAEA (Bauerfeind et al., 2014).
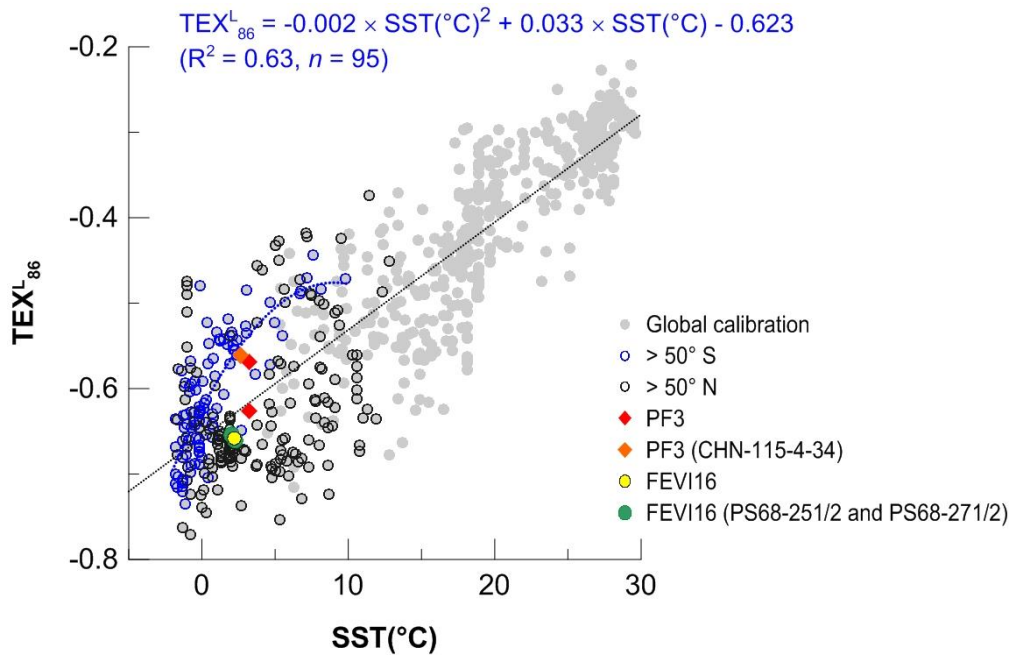
Figure 9. Correlation of TEX_{86}^L values with mean annual SSTs in the global ocean (gray symbols; Tierney and Tingley, (2015) and reference therein). Blue and black round symbols represent the high latitude regions higher than 50° S and 50° N, respectively. In the southern regions (>50° S), TEX_{86}^L values have a polynomial correlation with maSSTs (R^2 = 0.63, n = 95). Red and orange diamonds represent the flux-weighted mean TEX_{86}^L of the two traps at the site PF3 and TEX_{86}^L on the surface sediment (CHN-115-4-34), respectively. Yellow and green round symbols represent the flux-weighted mean TEX_{86}^L at the site FEVI16 and TEX_{86}^L on the surface sediments (PS68-251/2 and PS68-271/2), respectively.

Appendix A.

Table A1. Index values for assessing the terrestrial and/or methanogen GDGT inputs at FEVI16 and PF3 sediment traps. The exact sampling interval of each sample number at FEVI16 and PF3 can be found in PANGAEA (https://doi.pangaea.de/10.1594/PANGAEA.897268).

Cup no.	FEVI16				PF3							
	(1296 m)				(614 m)				(3196 m)			
	BIT [a]	MI [b]	%GDGT-0 [c]	|ΔRI| [d]	BIT	MI	%GDGT-0	|ΔRI|	BIT	MI	%GDGT-0	|ΔRI|
1	0.01	0.09	60	0.15	0.00	0.15	58	0.05	0.00	0.34	62	0.23
2	0.01	0.11	60	0.22	0.02	0.14	58	0.08	0.00	0.30	61	0.17
3	0.01	0.11	60	0.21	0.00	0.14	64	0.24	0.00	0.21	58	0.09
4	0.01	0.10	60	0.20	0.00	0.16	61	0.16	-	-	-	-
5	0.01	0.11	61	0.30	0.00	0.19	62	0.17	0.00	0.22	58	0.06
6	0.01	0.10	60	0.23	0.00	0.15	63	0.19	0.00	0.21	56	0.05
7	0.01	0.11	60	0.23	0.00	0.20	65	0.24	0.00	0.19	55	0.08
8	0.01	0.11	60	0.09	0.00	0.19	60	0.08	0.00	0.21	56	0.01
9					0.00	0.19	62	0.16				
10	0.01	0.13	61	0.14	0.00	0.23	64	0.20	-	-	-	-
11					0.00	0.20	59	0.06	-	-	-	-
12	0.01	0.15	59	0.19	0.00	0.21	64	0.26	-	-	-	-
13	0.01	0.13	59	0.10	0.00	0.21	62	0.19	-	-	-	-
14					0.00	0.16	61	0.16	-	-	-	-
15	0.02	0.14	59	0.13	0.00	0.15	60	0.15	-	-	-	-
16	0.02	0.13	61	0.22	0.00	0.14	60	0.11	0.00	0.21	56	0.04
17	0.01	0.11	61	0.20	0.00	0.16	62	0.16	-	-	-	-
18	0.01	0.09	63	0.26								
19	0.01	0.10	64	0.31								
20	-	-	-	-								
	Total 20 samples				Total 17 samples							

[a]: BIT (Hopmans et al., 2004; Weijers et al., 2006) for terrestrial input when > 0.3
[b]: MI (Zhang et al., 2011) for methanotrophic archaeal input when > 0.5 and normal oceanic signal when < 0.3
[c]: %GDGT-0 (Blaga et al., 2009; Inglis et al., 2015) for methanogenic archaeal input when > 67 %
[d]: \|ΔRI\| (Zhang et al., 2016) for both methanotrophic archaeal and terrestrial input > 0.3